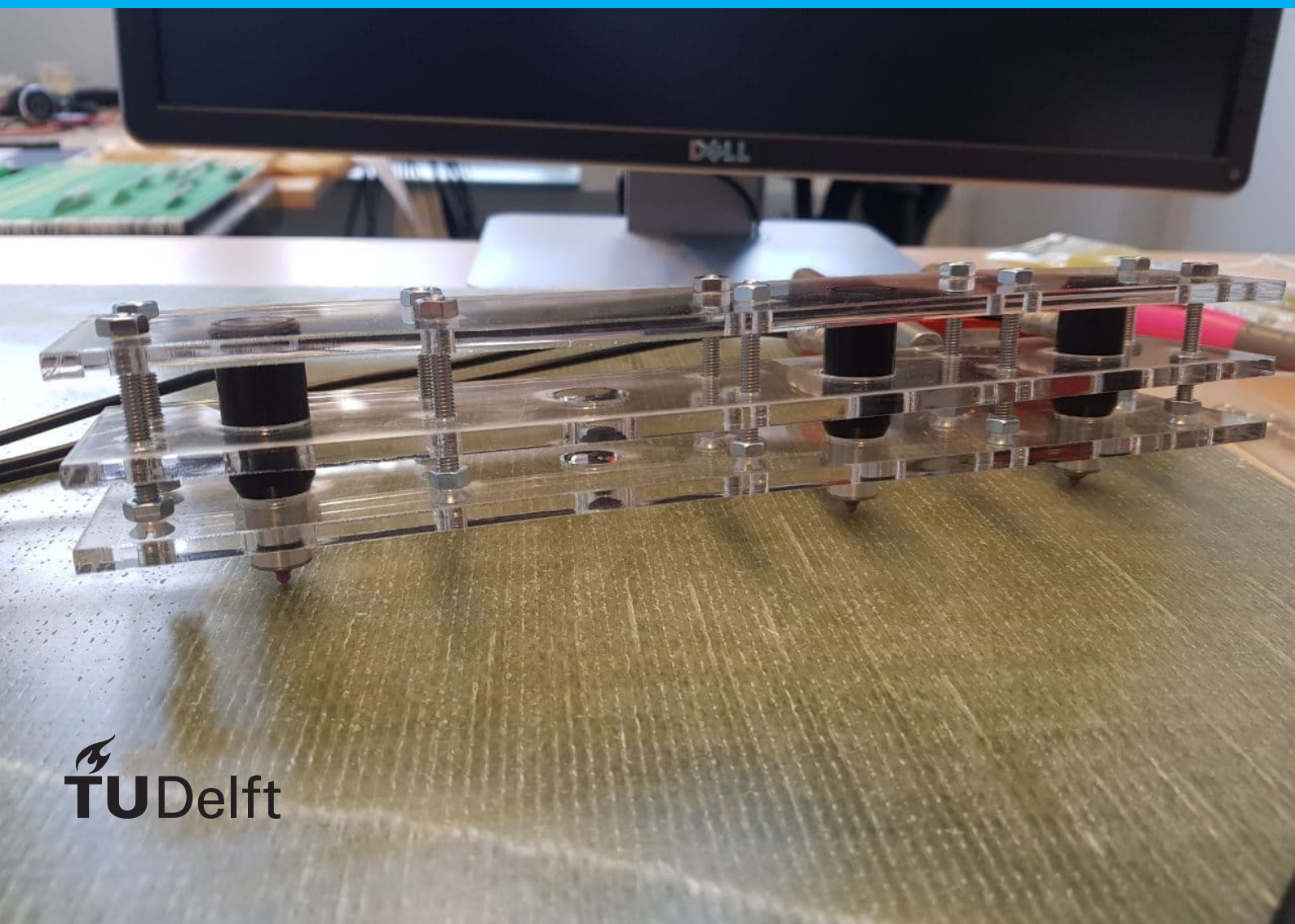


Feasibility evaluation of a non-destructive estimation of material properties of FRC structures using ultrasonic guided waves

Arnout W. Zaal



Feasibility evaluation of a non-destructive estimation of material properties of FRC structures using ultrasonic guided waves

by

Arnout W. Zaal

to obtain the degree of Master of Science
at the Delft University of Technology,
to be defended publicly on Friday May 7, 2021 at 10:00 AM.

Student number:	4384288	
Project duration:	March , 2020 – May, 2021	
Thesis committee:	Dr. C.L. Walters,	TU Delft, chair
	Dr. L. Pahlavan,	TU Delft, supervisor
	Prof. Dr. C. Kassapoglou,	TU Delft
	Ir A.J. Huijer MSc,	TU Delft

An electronic version of this thesis is available at <http://repository.tudelft.nl/>.

Abstract

Variations in the production process of fiber-reinforced composite (FRC) materials often influence the material properties of the end product more substantially than their metallic counterparts. It can be valuable for the structural performance and reliability to have a better estimation of the properties of the FRC after production. Detecting these material properties is often performed by intrusive or destructive testing, which are not desirable for in-situ applications. Samples are commonly taken from the material for mechanical testing and material characterization in the laboratory.

Feasibility of a non-destructive in-situ assessment method based on ultrasonic guided waves for estimation of the material properties of FRCs, e.g. stiffness in different directions, is investigated in this research. A portable and easy-to-apply measurement system is proposed that can also be less sensitive to the environmental conditions.

Point-contact transducers containing a piezoelectric material are utilized for measuring guided waves that propagate through the material. The dispersion characteristics, i.e. phase speed and group speed, of these guided waves are dependent on the layup of the fibers, thickness, and ply properties. Information about the group speed from multiple directions are extracted and compared with the group speeds obtained using a semi-analytical method. A genetic algorithm (GA) is implemented to minimize the difference between the measured and modeled group speeds and obtain the ply properties. The methodology was applied to five glass FRC laminates with different layups. In the numerically simulated case, the error in the estimated material properties turned out to be less than 12%. The coefficient of variation in the experimental results of stiffness values was also less than 20%.

The results suggest that the proposed combination of point contact transducers, analysis of group speeds, and GA optimization procedure can potentially form a viable approach for in-situ assessment of material properties of FRCs.

Preface

This research is conducted to obtain the degree 'Master of Science' at the TU Delft as part of the study Marine Technology. This research proposes a method to non-destructively estimate material properties of a composite plate. This is a crucial step between the optimization of a design and the assumptions that are made about material properties of the material. Experiments with guided waves, too small to see and too weak to feel, offer an informative insight into the applications of guided waves.

I want to thank the many people that helped me during these crazy times. In the first place, my supervisors Pooria Pahlavan and Arno Huijser. Your knowledge, experience, and always positive attitude will always be remembered. During all those Skype meetings, drawing on a whiteboard, or assisting with the new experimental equipment has been a joy every day. Furthermore, I would like to thank my committee members for their assessment of the work.

Help en motivation from the close friends and family around me has been really appreciated. I especially want to thank my girlfriend Anna-Louise and my housemates during lockdown: Otto and Stefan. Finally, I want to thank my family: Ingrid, Fred, Isabelle, Valerie, and Matthijs. All of which worked hard for themselves but were also great support for others.

*Arnout Zaal
Delft, May 2021*

Contents

Abstract	iii
Preface	v
List of Tables	ix
List of Figures	xi
Nomenclature	xiii
1 Introduction	1
1.1 State of the Art	1
1.2 Problem Statement	2
1.3 Research Question	2
1.4 Outlining of Research	2
2 Methodology	5
2.1 Analysis of Guided Waves	5
2.1.1 Determination of Dispersion Curve	5
2.2 Signal pre-processing	8
2.2.1 Defining a Source Signal	8
2.2.2 Applying a Time Window	8
2.2.3 Improving the Signal-to-Noise Ratio	9
2.2.4 Simulation of Sensor Signals	9
2.3 Time of Flight Extraction	10
2.3.1 Selection of Time of Flight	10
2.4 Material Estimation Method	13
2.4.1 Error Description	13
2.4.2 Optimization Algorithm	15
3 Experiments	17
3.1 Plate Specifications	17
3.2 Experiment setup	20
3.3 Point contact transducer	23
3.3.1 Sensor holder	23
3.3.2 Settings and Reflecting Waves	24
4 Results and Discussion	27
4.1 Sensitivity Analysis	27
4.1.1 Effect of Changing Material Properties	27
4.1.2 Effect from Production Errors	30
4.1.3 Accuracy of the Minimization Algorithm	31
4.2 Results for Simulated Signals	32
4.3 Measured Results	36
4.4 Results from Experiment	39
4.4.1 Simulated Results	39
4.4.2 Measured Results	40
5 Conclusion & Recommendations	43
Bibliography	45

List of Tables

2.1	Settings for a genetic algorithm	16
2.2	Parameters for a genetic algorithm	16
3.1	Material name	17
3.2	Material properties	17
3.3	Ply stacking sequence	18
3.4	Waveform Generator Settings	25
3.5	Data Acquisition Settings	26
4.1	Material Properties	27
4.2	Dispersion speed along fiber direction with material parameters at · 70 %	29
4.3	Dispersion speed along fiber direction with material parameters at · 130 %	29
4.4	Dispersion speed perpendicular to the fiber direction with material parameters at · 70 %	30
4.5	Dispersion speed perpendicular to the fiber direction with material parameters at · 130 %	30
4.6	Function score · 1000	31
4.7	Estimation of Young's modulus E_1	31
4.8	Estimation of Young's modulus E_2 & E_3	31
4.9	Estimation of Poisson's ratio ν_{23}	32
4.10	Estimation of the Shear modulus G_{12}, G_{13}	32
4.11	Estimation of the Shear modulus G_{23}	32
4.12	Material estimations of iterations with longest optimization	32
4.13	Material properties in the numerical simulation	33
4.14	Function score of simulated signals	35
4.15	Plate material genetic algorithm of simulated data with fixed density and narrow Poisson's	39
4.16	Function score of simulated signals	39
4.17	Plate material genetic algorithm of measured data with fixed density and narrow Poisson's	41
4.18	Function score of measured signals	41
4.19	Estimation of material properties	41

List of Figures

1.1 Steps in the proposed approach for estimation of material properties	3
2.1 Material Properties Roadmap	5
2.2 Phase dispersion speed	6
2.3 Group dispersion speed	6
2.4 Wavelength-frequency without selection of order	7
2.5 Wavelength-Frequency with selection of order	8
2.6 Source Signal with center frequency of 70 kHz	8
2.7 Signal with different noise levels	9
2.8 Measured signal before and after averaging	9
2.9 Measured Source Signal	10
2.10 Selecting individual signals from measured data	10
2.11 Selecting individual signals from simulated data	11
2.12 Separated signals	11
2.13 Peak amplitude of separated wave	11
2.14 Measured Propagation Speed	12
2.15 Polynomial fit from measured data	13
2.16 Polynomial fit from measured data	14
2.17 Children in a genetic algorithm	15
3.1 Layups	18
3.2 Production of the plates	19
3.3 Flow of resin	19
3.4 Resin used in production the plates	20
3.5 Measurement system	20
3.6 Waveform generator	21
3.7 High voltage amplifier	21
3.8 Vallen transducer	21
3.9 Pre-amplifiers	21
3.10 Frequency response	22
3.11 Data acquisition system	22
3.12 Cone closeup	23
3.13 Sensor holder	24
3.14 Close up of sensor holder	24
3.15 Sensor Setup	25
3.16 Conic sensor on plate	25
4.1 Fiber direction	28
4.2 Dispersion Curve at 0°	33
4.3 Dispersion Curve at 90°	33
4.4 Dispersion Speed at 60 kHz	34
4.5 Source Signal	34
4.6 Simulated signal from sensors	34
4.7 Group speed extraction of simulated signals	35
4.8 Group speed extraction of simulated signals	35
4.9 Polynomial fit through the predicted group speeds	36
4.10 Cross correlation of extracted group speed	36
4.11 Unedited measurement	37
4.12 Measured group speed with polynomial curve	37

4.13 Measured group speed with polynomial curve	38
4.14 Measured and optimized polar plot of plate 1	38
4.15 Correlation between measured and expected results	39
4.16 Measured group speed with polynomial curve	40
4.17 Measured group speed with polynomial curve	40

Nomenclature

ν	Poisson's ratio
ρ	Density
θ	Layup
B	Maximum frequency
c_g	Group Speed
c_p	Phase Speed
E	Young's Modulus
f_s	Sample Rate
G	Shear Modulus
N_{dB}	Amplification Factor
t	Specimen thickness
V_{in}	Input Voltage
V_{out}	Output Voltage
AE	Acoustic Emission
B	Sample Bandwidth
DAS	Data Acquisition System
DPT	Dry-point-contact
FRC	Fiber reinforced composite
GA	Genetic Algorithm
TOF	Time of Flight
TR	Transient Recording
VOC	Coefficient of Variation

Introduction

There are many factors that can influence the material properties of composite materials, such as the production process variations or in-service loads and degradation. Determining these material properties e.g. stiffness of a material, is often performed by intrusive or destructive testing [Ammar et al., 2019, Carlsson et al., 2014, Egorikhina et al., 2015, Jenkins, 1988, Munoz et al., 2015]. Such testing can result in accurate properties estimations. Bending or tension tests on a piece of material is fairly straightforward and standardized. The disadvantage is however a damaged material. One will therefore always have to deal with uncertainty in the material properties as long as the material has not been sampled destructively and tested [Dey et al., 2018]. Non-destructive testing can potentially be performed using ultrasonic guided waves [Lamb, 1917]. Guided waves are ultrasonic waves that are bounded by the dimensions of the structure. Guided waves are utilized in diverse applications of non-destructive testing such as beams [Ghadami et al., 2018], plates [Ihn and Chang, 2008, Kundu et al., 2007, Salmanpour et al., 2016, Xie et al., 2019], pipes [Alleyne et al., 2001, Kim et al., 2013, Mencik and Ichchou, 2007, Nagy et al., 2014], conical shells [Li et al., 2012, Sun et al., 2017], bolts [Beard and Lowe, 2003], train tracks [Hayashi et al., 2005], and pressure vessels [Li et al., 2015].

Guided waves are measured for their specific propagation speed at different frequencies. The measurements are subsequently processed [Bellanger, 2001, Gruber and Hayes, 1997, Malocha, 2018]. Analysis of these measurements will give information about the group speed of relevant mode shapes [Darnton and Ruzzene, 2017, Moilanen et al., 2006, Yen and Lin, 2000, Zhao et al., 2014].

This research focuses on the material characterization of thin fiber-reinforced composite (FRC) plates using guided waves. Guided waves are influenced by material properties, dimensions, and layup of the structure. The group speed of guided waves can be obtained experimentally and used for estimation of the material properties without intrusive experiments.

A genetic algorithm optimization method will vary material properties to minimize the error between the measured wave speeds and wave speeds corresponding to semi-analytical models using a similar geometry composite plate.

1.1. State of the Art

NDT characterization of material properties using a GA has been performed by Ragauskas and Belevicius [2009]. Global eigenfrequency vibrations are determined to identify material properties of unidirectional specimen. The accuracy of the estimation is as good as 0.1 %. The material properties do however depend on the dimensions of the specimen. Shape optimization of the specimen is needed to achieve the desired accuracy. Accuracy without this optimization can be between 10 % and 40 %.

Marzani and De Marchi [2012] describe a procedure using a GA that updates unknown material properties and compares them with a semi-analytical finite element method. This method is tested using pseudo-experimental data which is obtained by adding Gaussian noise to simulated tie-wave forms. The stiffness properties are identified to have a maximum mean error of 8 %.

Vishnuvardhan et al. [2007] propose an array of piezoelectric-based transducers. The sensors are used to reconstruct elastic properties, and compare the results with a laser-based system and theoretical estimates.

Kersemans et al. [2014] utilize a pulsed ultrasonic polar scan as a solution to the complexity of the data acquisition and the extensive post-processing in conventionally used systems. Ponschab et al. [2019] use a laser vibrometer to measure guided waves and reconstruct elastic constants using an inverse characterization. The method is successfully shown with simulated data, but appropriate measurement data could not be retrieved because of changing conditions.

The state-of-the-art research use equipment which is impractical for use in-situ. In the research, it is therefore proposed to use point-contact piezoelectric transducers. Piezoelectric transducers are used to measure the guided waves. Although conventional piezoelectric transducers are widely used, it is remarked that point-contact transducers have clear advantages. They are versatile, easy to use and can be placed without couplant material [Rus et al., 2007].

Most point-contact transducers use a point contact with a ceramic contact point [Lu and Xu, 2011, Rus et al., 2005]. Although there is research done to point-contact transducers using a piezoelectric contact point [Hutchins et al., 1989, Sause et al., 2012], the design of the contact point influences the transfer of energy by the transducer [Fraser et al., 1978, Sause et al., 2012, Zul Karnain and Rajagopal, 2020], the effect of roughness of the material on the transfer function is described by Tressler et al. [1998], and Baik and Thompson [1984], point-contact transducers have not been used in the described NDT application. This topic is an original contribution of this research and is believed to have important practical implications.

1.2. Problem Statement

The current knowledge about characterizing material properties based on guided waves has been shown to work well in existing research. Notable in this type of research is the method of collecting signals. The method for measurement data has drawbacks which ranges from long testing periods, sensitively to change of environmental conditions, and no portable options. It is therefore hard to use these type of systems in a mobile and easy-to-tune configuration. The gap in the current knowledge is a method that is more portable and applicable for in-situ use. This can be solved by using point-contact piezoelectric transducers. These transducers can be used both as actuators and sensors on the composite plate.

Furthermore, there is a need for further experimental demonstration of the feasibility of estimating material properties of FRC with larger thickness, as is common in maritime applications. Most of the existing publications deal with very thin thicknesses.

1.3. Research Question

The goal of this research is to estimate the material properties of FRC laminates using an array of easy-to-mount sensors that can be placed on a FRC plate. The array will pulse and measure guided waves, followed by a prediction of the material properties. This method should be independent of environmental changes and should not require preparation of the composite plate itself.

The main question is if material properties of fiber-reinforced composite can be estimated non-intrusively and non-destructively using guided ultrasonic waves using point-contact transducers? This question can only be solved if the three other sub-questions can be answered as well.

The first step in this process is measuring the relevant guided waves. Can guided waves be measured by NDT performed on a FRC plate, with clear data and at the relevant frequency?

The second question is related to the development of a method to extract the relevant wave modes. There are many guided wave modes. Can the relevant wave modes be detected, and can the group speed of these waves modes be extracted from the data?

The third research question is if an inverse procedure can be developed that can take the group speed of the relevant wave modes of ultrasonic guided waves, and translate that to material properties?

1.4. Outlining of Research

The research focuses on assessing the feasibility of building a method that can estimate material properties of FRCs based on guided waves. The steps necessary for this research are shown in Figure 1.1. The method is applied to both fully simulated data and experimental data.

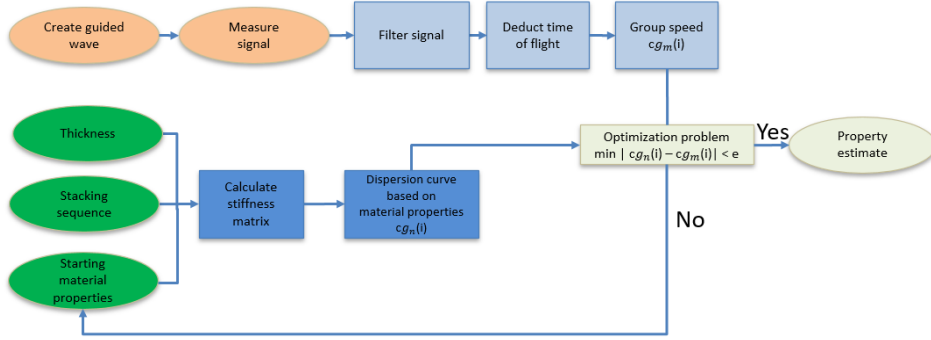


Figure 1.1: Steps in the proposed approach for estimation of material properties

Chapter 2 describes the method estimating material properties by comparing the group speed of different wave modes of guided waves with the group speed based on a semi-analytical method. This is an optimization problem that is solved iteratively in the white block in the figure. Before that, the raw data from the experiment is processed and filtered. The group speed of specific wave modes is extracted and applied as input to the optimization problem. The model can simulate the experimental data with information about the dispersion curve based on the semi-analytical method. In Chapter 3, the experimental setup that creates and measures guided waves using point-contact transducers is described. Chapter 4 shows the results from the experiment and the solution to the optimization problem. The thesis finishes with conclusions and suggestions for possible future work.

2

Methodology

This chapter will describe the methodology for estimations of material properties of FRCs based on experimentally acquired guided waves. That will start with section 2.1 describing the estimation of the group speed based on input parameters such as the material properties. Section 2.2 will prepare the raw data for further analysis. Section 2.3 encompasses the speed of different modes of guided waves which is extracted from the pre-processed data. Section 2.4 presents the iterative process that varies the starting material properties in an error minimization process. The measurement of the signals is described in Chapter 3.

2.1. Analysis of Guided Waves

The analysis of the guided waves will result in a dispersion curve based on basic mechanical material properties and geometry. The process starts with subsection 2.1.1 where the group speed will be estimated using a semi-analytical approach proposed by Pahlavan [2012]. Next, section 2.2 describes multiple pre-processing steps. The third section of this chapter shows how the time of flight is determined. Finally, section 2.4 describes the method by which the difference between measured group speeds and estimated group speeds is quantified and minimized.

2.1.1. Determination of Dispersion Curve

The calculation of the dispersion speeds of guided waves are crucial for the prediction of material properties. The roadmap that describes this step is shown in figure 2.1. One starts with calculating the stiffness matrix based on model parameters such as plate thickness, stacking sequence, and material properties.

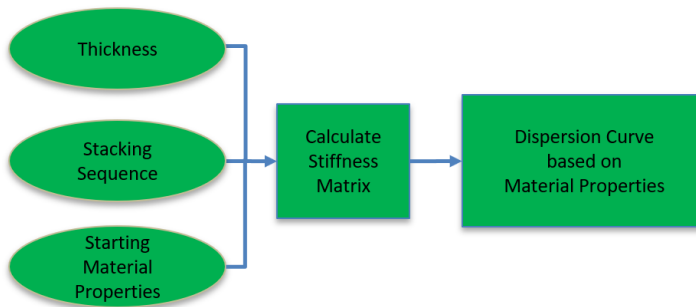


Figure 2.1: Material Properties Roadmap

Calculation of both the stiffness matrix and the dispersion curves resulting from the stiffness matrix can be determined using numerical and semi-analytical methods e.g. finite element method [Mace et al., 2005, Rose, 2014], spectral element method [Ostachowicz et al., 2012, Sun et al., 2017], spectral finite element method [Gopalakrishnan et al., 2008], semi-analytical finite element method [Barouni and Saravanos, 2016, Gresil and Giurgiutiu, 2013, Zuo et al., 2017], and boundary element method [Gravenkamp et al., 2012].

The semi-analytical approach uses a discretized domain through the cross section and an analytical approach for the direction of the wave propagation. In this thesis, the method presented by Pahlavan [2012] is used for obtaining the dispersion curves, as briefly described below

The governing equation is presented in Equation 2.1. In this equation, u denotes the displacement field in 3D, \ddot{u} denotes the corresponding accelerations, ρ is the density, σ is the stress tensor, and f denotes the external force vector.

$$\nabla \cdot \underline{\sigma} + \mathbf{f} = \rho \ddot{u} \quad (2.1)$$

$$\hat{u}_n = \hat{U}_n(z) \exp \left(i \left[\omega t - \left(k_x^n x + k_y^n y \right) \right] \right) \quad (2.2)$$

Where $\hat{U}_n(z)$ is a vector of displacement functions in the thickness direction that have to be determined using the boundary conditions. These boundary conditions create the effect of the previously described guided waves. Free surface boundary conditions are applied i.e. $\sigma_{zz} = 0, \tau_{zx} = 0, t_{zy} = 0$, with z -directions being the thickness direction. The wavenumbers (k_x, k_y) are obtained for a given frequency (ω) and in the x - and y -directions of propagation. The wave-number in the direction of wave propagation is therefore:

$$k_n = \sqrt{k_x^2(\omega_n) + k_y^2(\omega_n)} \quad (2.3)$$

The relationship between the wavenumber, wavelength, and wavenumber is as follows:

$$k_n = \frac{2\pi}{\lambda_n} = \frac{\omega_n}{c_p^n} \quad (2.4)$$

Furthermore, the group speed can be estimated once the relationship between wavenumber and frequency is known.

$$c_g^n = \frac{\partial \omega_n}{\partial k_n} \quad (2.5)$$

For more details on the numerical implementation and solution of the method, the reader is referred to Pahlavan [Pahlavan, 2012]. The eigenvalue problem is solved for every frequency. An example of the resulting dispersion curves are shown in Figure 2.2 and Figure 2.3. The material properties used for this figure are: $E_{11} = 46.2$ GPa, $E_{22} = E_{33} = 13.1$ GPa, $G_{23} = 5.1$ GPa, $G_{12} = G_{13} = 4.1$ GPa, $\nu_{13} = \nu_{23} = 0.29$, and $\nu_{23} = 0.28$. The density is 1872 kg/m^3 , the thickness is 9.2 mm , and the direction of travel is along the fiber direction of the layup which is $[0]_8$.

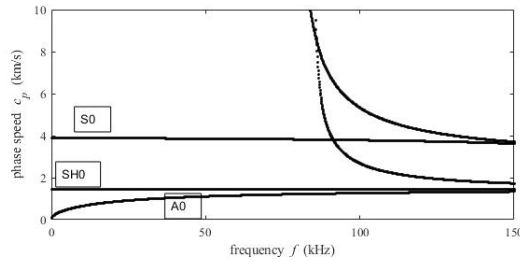


Figure 2.2: Phase dispersion speed

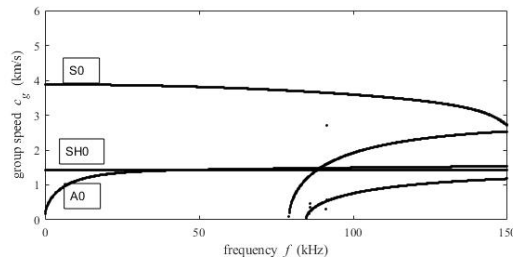


Figure 2.3: Group dispersion speed

Material Properties

A key question in this research is that how material properties influence the dispersion characteristics of the composite plate. This research will primarily focus on the Young's Modulus (E), Poisson's ratio (ν) and the Shear Modulus (G). The described parameters are shown in Equation 2.6.

$$\mathbf{Mat} = [E_{11}, E_{22}, E_{33}, \nu_{12}, \nu_{13}, \nu_{23}, G_{12}, G_{13}, G_{23}] \quad (2.6)$$

This gives 9 individual material properties. However, because of Hooke's law, orthogonal ply's can be described using 5 individual properties. These relations can be described by Equation 2.7, Equation 2.8 and Equation 2.9. The eventual material properties of the composite plate are therefore described by equation Equation 2.10.

$$\frac{E_2}{\nu_{12}} = \frac{E_3}{\nu_{13}} \quad (2.7)$$

$$G_{12} = G_{13} \quad (2.8)$$

$$G_{23} = \frac{E_2}{2(1 + \nu_{23})} \quad (2.9)$$

$$\mathbf{Mat} = [E_{11}, E_{22}, \nu_{12}, \nu_{23}, G_{12}] \quad (2.10)$$

Selection of the correct dispersion curve

The equation of motion can have multiple solutions for every frequency, in an eigenvalue form. These solutions describe different wave modes. The solutions can be ordered by wavelength from small to big. The relation between wavelength and frequency as described by Equation 2.11 is visualized in Figure 2.4.

$$f_p^n = \frac{\omega_n \cdot \lambda_n}{2\pi} \quad (2.11)$$

Improper ordering of the eigenvalues results in crossing wave modes. Proper separation of wave modes is needed in order to numerically calculate the group speed.

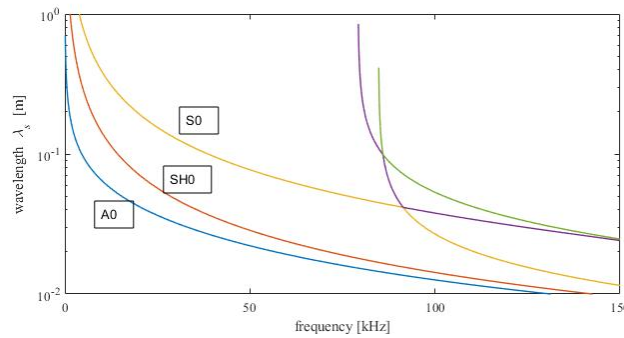


Figure 2.4: Wavelength-frequency without selection of order

The selection of the points belonging to the same wave mode is performed by using a finite backward difference method. The finite backward difference method is based on a second-order Taylor polynomial described by Equation 2.12. The first-order and second-order differential are described by Equation 2.13 and Equation 2.14. The local truncation error in this approximation is third order.

$$f(t_n + h) = y(t_n) + f'(t_n)h + \frac{1}{2}h^2 f''(t_n) + O(h^3) \quad (2.12)$$

$$f'(t_n) \approx \frac{f(t_n) - f(t_n - h)}{h} \quad (2.13)$$

$$f''(t_n) \approx \frac{\frac{f(t_n) - f(t_n - h)}{h} - \frac{f(t_n - h) - f(t_n - 2h)}{h}}{h} = \frac{f(t_n) - 2f(t_n - h) + f(t_n - 2h)}{h^2} \quad (2.14)$$

Estimations of $f(t_n + h)$ of every row is determined and allocated to their respected curve. This results in the curves as are shown in Figure 2.5. This creates the opportunity to 'follow' each wave mode from its respective starting point in the frequency domain.

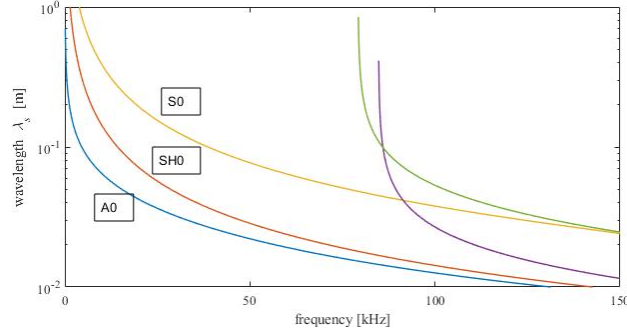


Figure 2.5: Wavelength-Frequency with selection of order

2.2. Signal pre-processing

This chapter includes the definition of the source signal that is created by the waveform generator. But it will also include the shift of a signal in time, filtering a signal for a specific frequency and windowing.

2.2.1. Defining a Source Signal

In order to generate guided waves, a Hanning- windowed sinusoidal burst signal is used in this research. The Hanning window is described in Equation 2.15.

$$\omega_n = \frac{1}{2} \left[1 - \cos\left(\frac{2\pi n}{N}\right) \right] \quad (2.15)$$

Where $N+1$ is the length of the signal. The burst signal is defined as:

$$s(t) = \left[\left(1 - \cos(2\pi(t - \Delta t)) \right) * \left(\sin(2\pi * F_c(t - \Delta t)) \right) \right]_0^{\frac{n_p}{f_c}} \quad (2.16)$$

A source signal with $N=5$ and center frequency of 70 kHz is shown in Figure 2.6.

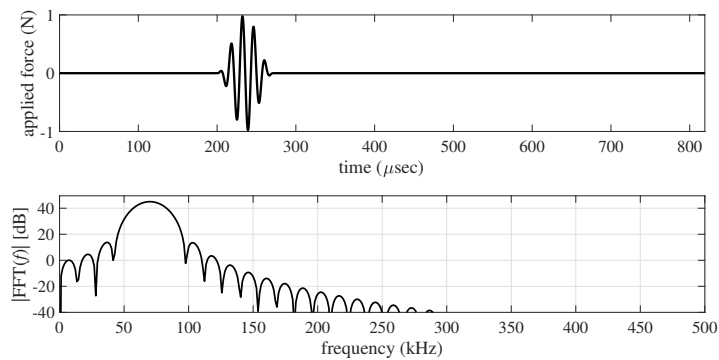


Figure 2.6: Source Signal with center frequency of 70 kHz

2.2.2. Applying a Time Window

Not every part of a transient recording is relevant for analysis of the guided waves, for example due to boundary reflections and mode conversions. In this research, a window around the expected arrival time will be applied over the transient recording such that only the relevant part of the guided wave is preserved.

2.2.3. Improving the Signal-to-Noise Ratio

The first step of filtering the noise is performed by averaging multiple signals measured. These signals need to be taken in the same experiment as a small time-shift in the signal can influence the average of the signal significantly. Averaging the signal is mainly effective against random white-noise. The averaging of the signal for every individual direction of the experiment is shown in Equation 2.17.

$$S_{avg}(t) = \frac{1}{N} \sum_{n=\langle N \rangle} S_n(t) \quad (2.17)$$

The definition of S in this equation is the voltage measured by the receiving transducers at time t . The averaging of the signal is performed for every time point. The total amount of signals is defined as N . The expected reduction in noise is described by Mark and Workman [Mark and Workman, 2018]. The amount of white noise is reduced by a factor 2 for when the number of scans is doubled.

The effect of averaging multiple signals is shown in Figure 2.7. Figure 2.7a an example sinusoidal wave represented by the blue data. The orange data shows only the level of normal distributed noise in the signal. It is visually clear to see that the amount of noise decreases significantly in Figure 2.7b and Figure 2.7c. A remark must be made that there will be an optimum between the amount of signals measured, the decrease in noises and the measurement time.

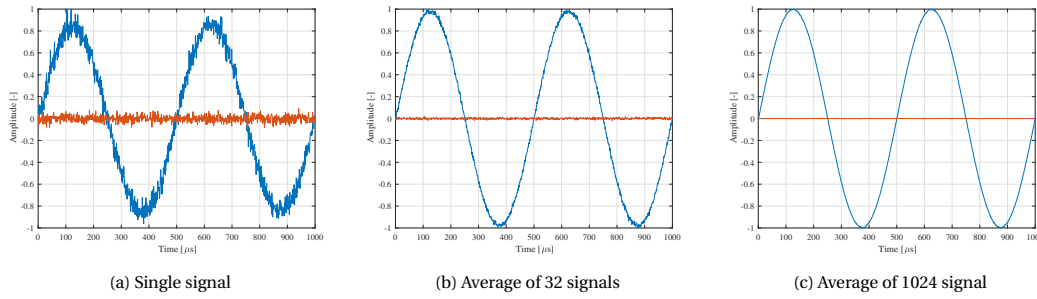


Figure 2.7: Signal with different noise levels

The method of averaging applied to actual data is shown in Figure 2.8. A significant improvement can be observed in the level of noise. This has been achieved with the use of 32 individual signals.

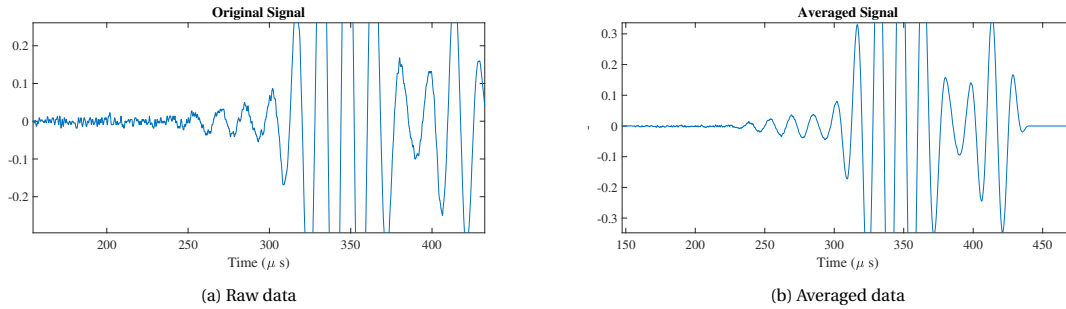


Figure 2.8: Measured signal before and after averaging

2.2.4. Simulation of Sensor Signals

The propagation time of a signal is determined by the group speed of every mode, distance, and frequency. The dispersion curve described in subsection 2.1.1 is used to determine the group speed. The distance between source signal and receiving transducer is equal to the distance used in the experiment.

Simulation of the signal creates the possibility to exclude external factors such as error in the measurement location, discrepancies in the material properties, and direction of fibers. Also, there are no boundary reflections implemented in this model. The shift in time is performed in the frequency domain as shown in Equation 2.18. The time shift $s(n - \Delta)$ is applied in the frequency domain. This is performed with a phase shift ($e^{-j\omega_k \Delta}$) applied to signal $S(\omega_k)$.

$$s(n - \Delta) \longleftrightarrow e^{-j\omega_k \Delta} S(\omega_k) \quad (2.18)$$

2.3. Time of Flight Extraction

The estimation of material properties is based on the dispersion curve of guided waves. Ideally, one would like to retrieve the group speed of as many different guided wave modes as possible. However, higher-order wave modes are typically of very small amplitude and difficult to measure reliably, higher-order wave modes are therefore preferably not actuated. The focus of this research is therefore on zero-order antisymmetric (A_0) and zero-order symmetric guided wave modes (S_0).

The method to determine the time of flight of different type of guided waves is discussed in Chapter 2.3.1. This is part of the proposed method in Figure 1.1, as illustrated in Figure 2.9



Figure 2.9: Measured Source Signal

Every step of the experiment influences the eventual measurement of the emitted wave such as the amplifiers, transducer, and attenuation and dispersive character of FRCs and cables. The result of this process is the raw data, of which the analysis is now described.

2.3.1. Selection of Time of Flight

This section will show the first selection of signals in a defined time frame before applying a frequency filter for analysis of the envelope of the signal. The equipment used in this experiment is described in Chapter 3. The distance between the source and the sensors is 60 mm each, which results in a distance of 240 mm between the actuator and the furthest sensor from the source. This creates a separation between the arrival of different types of guided waves, which travel at different group speed because of their dispersion character. The measured signal is filtered in the frequency domain with a width of 40 kHz. A more narrow filter range has shown instability.

The measured data is separated before information about individual waves is extracted. The selection of the signals starts with detection of the maximum amplitude. This window is selected by the width of the generated guided wave, minus $5 \mu s$ in advance and $15 \mu s$ on the later side of the signal. The second window is generated from $100 \mu s$ to the peak amplitude, minus the width of the wavelet, plus an additional $5 \mu s$. The highest amplitude in the measures voltage is the antisymmetric wave. This point is the starting location from where the split of the signal will be determined. This point in time is called $tp_{A0,n}$. The width on both sides of this point is l_w , which is half of the width of the wavelet that is created by the actuator. An additional shift in time is added as to give room for a transition in the window function. The window contributed to the first arriving wave is between ts_1 and ts_3 . The window of the second wave is bounded by ts_2 and ts_4 . A visual representation of these windows is shown in Figure 2.11 and Figure 2.10. The signal shown in Figure 2.11 is created by using the material properties shown in section 2.4, the source signal and method of simulating this signal over a distance of 0.24 m is described in section 2.2.

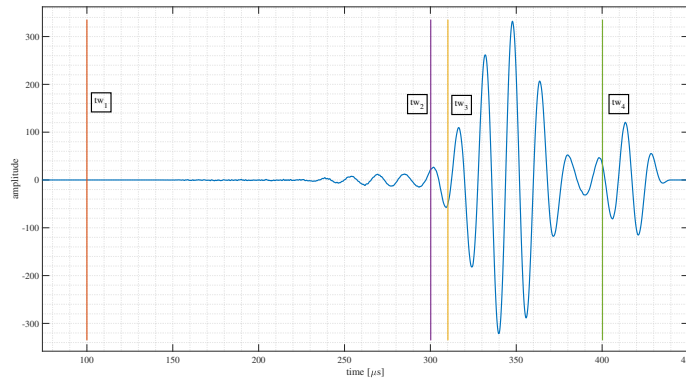


Figure 2.10: Selecting individual signals from measured data

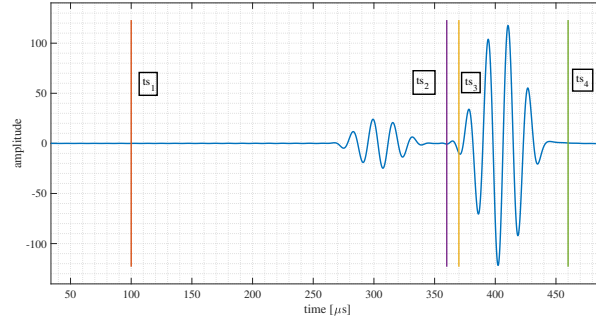


Figure 2.11: Selecting individual signals from simulated data

The window is applied using a flat top sinusoidal shape with a transition period of 10 % on both sides of the window. The results of this tool is shown in Figure 2.12.

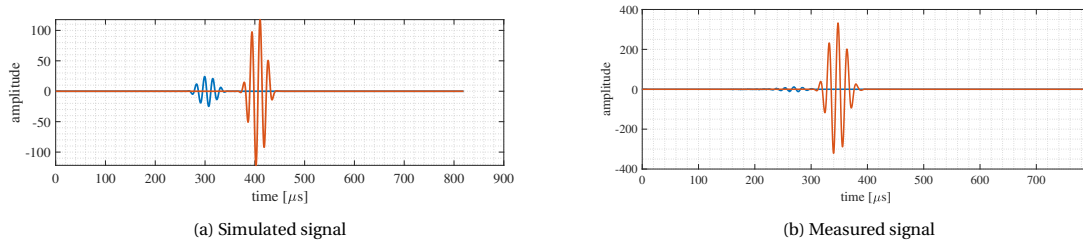


Figure 2.12: Separated signals

As the signals vary in amplitude, both wave modes been normalized. This is shown in Figure 2.13. The envelope of both waves shows the peak in the voltage that has been measured by the data acquisition system. These peaks are used to determine the time of flight of the signal.

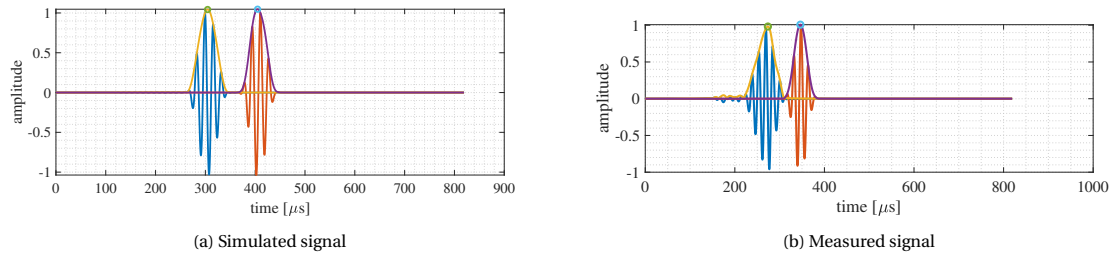


Figure 2.13: Peak amplitude of separated wave

The time of flight of the anti-symmetric wave and symmetric wave is determined by the peak amplitudes in the filtered signals and separated signals. This is shown in Equation 2.19 and Equation 2.20.

$$TOF_{A0} = tp_{A0,2} - tp_1 \quad (2.19)$$

$$cg_{S0} = \frac{1}{\frac{1}{cg_{A0}} - \frac{tp_{A0,4} - tp_{S0,4}}{d4}} \quad (2.20)$$

The peak amplitude of the filtered signal at the transducer closest to the source is tp_1 , $tp_{A0,4}$ is the peak amplitude of the antisymmetric wave at sensor 4, which is the furthest from the actuator. The group speed cg_{A0} is estimated by dividing the distance between both sensors with the time of flight TOF_{A0} . The group speed of the symmetric wave is based on the group speed of the anti-symmetric wave, plus the increase in speed measured because of the earlier arrival of the symmetric wave over the entire distance between actuator the sensor furthest from the source.

Results

The result of this method is shown Figure 2.14. 'Wave 1' relates to the propagation speed of the first peak amplitude and 'Wave 2' relates to the second peak with an amplitude of the antisymmetric wave which is significantly higher. The data used for this approach is acquired from plate 1. This plate is 10.2 mm thick and has a $[0_5 90_5]_s$ layup.

Giurgiutiu [2003] has shown that the transfer functions between transducers and plates for symmetric and anti-symmetric waves is also a function of frequency. Applying this theory can result in tuning of amplitudes of the symmetric and anti-symmetric guided waves.

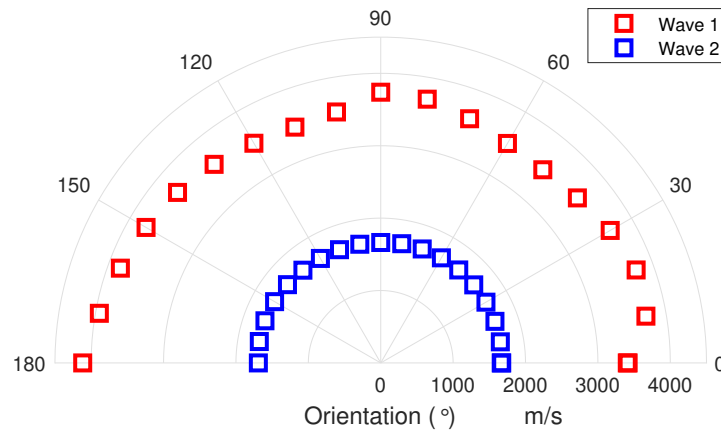


Figure 2.14: Measured Propagation Speed

2.4. Material Estimation Method

The goal is to acquire material parameters that result in a similar numerical dispersion curve as the dispersion curve based on measurements. The method on which the optimization problem is implemented will be elaborated here. Inspiration for the optimization of the material properties comes from Lee et al. [2014].

2.4.1. Error Description

An error function is applied such that the difference between semi-analytically determined group speeds of wave modes and measured group speed of wave modes are quantified. The error function is minimized in an optimization algorithm. This makes the function defining the error between these values an integral part of the optimization.

The group speed determined in subsection 2.3.1 contains a variability which occurs in the data acquisition phase and during the signal analysis. It must be prevented that the optimization is based on variability of individual calculation. A solution to this is fitting a function through all data points using a least-squares approach. This can reduce the effect of outliers in measured group speeds.

A method using a polynomial function is preferred as this function is compliant and does not call for individually tuned settings. A multitude of orders is shown in Figure 2.15. These options use Equation 2.21.

$$p(x) = p_1 x^n + p_2 x^{n-1} + \dots + p_n x + p_{n+1} \quad (2.21)$$

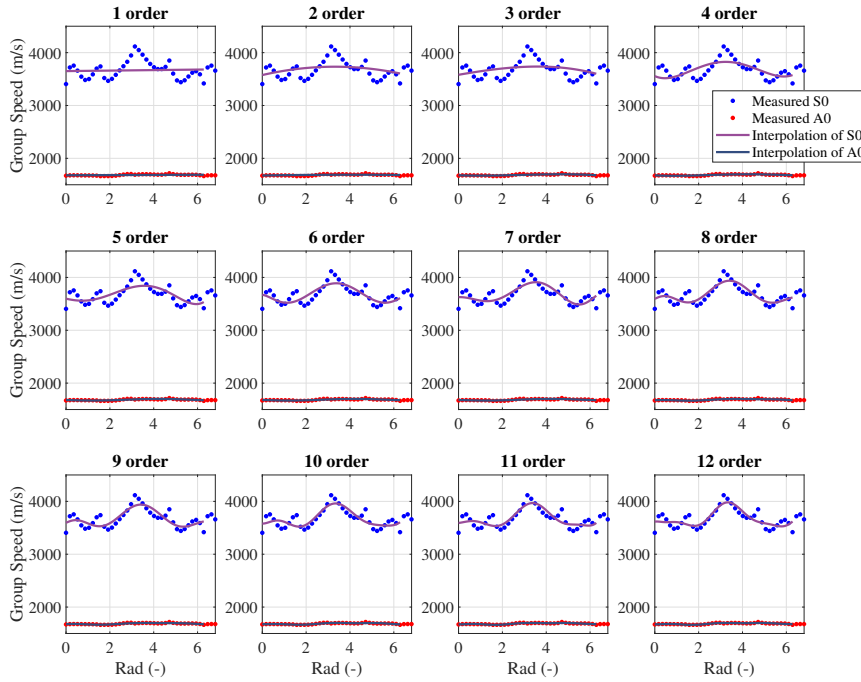


Figure 2.15: Polynomial fit from measured data

There is an increase in group speed of S0 waves, in plate 1 which has a layup of $[0_5 90_5]_s$. It seems that the higher the order of the polynomial used, the closer the interpolation is to the measured data. The order of the polynomial function is increased to improve the flexibility of the function, resulting in a lower average distance between the function and the measured group speeds.

Even though the general fit shows the group speed of the wave modes, it is not yet satisfactory to possible to describe all the relevant detail from the experiment. This is especially visible in the curve of the symmetrical wave. The peak of group speed at 3 rad is described by the function. There is however a deficiency in the description of speed increase from 0 to 1 rad. The fit passing the group speed of the antisymmetric wave is shown again in Figure 2.16. The increasing order of the fit results in a good fit with the data, while reducing the effect of outliers in the group speed estimation.

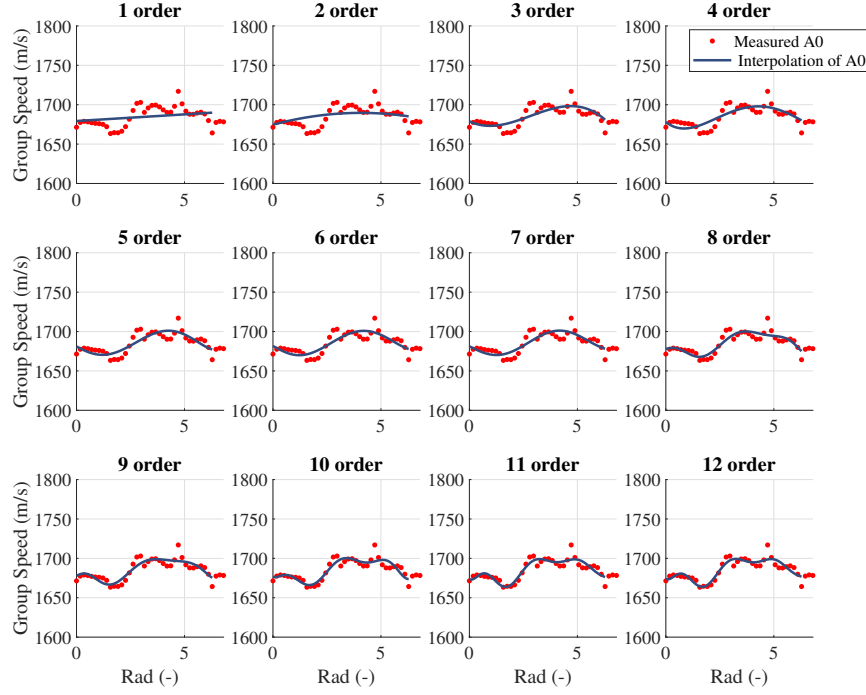


Figure 2.16: Polynomial fit from measured data

Since the projected curve based on experimental data is ultimately undesirable to describe the group speeds, a piece-wise polynomial fit is proposed next.

Piecewise Polynomial Fit

A piecewise polynomial fit is proposed that is described by 4 functions to describe the circumference per quarter, i.e., $[0, 80]$, $[90, 170]$, $[180, 260]$, and $[270, 350]$. The measurements in the experiment are performed at steps of 10° orientation around the source signal. As discussed, there can be variations in group speed estimations between angles, creating the requirement to decrease the effect of errors in individual orientations. The polynomial function is described in Equation 2.22. This is solved using matrices as described by Equation 2.23.

$$c_g(\phi) = p_1\phi^4 + p_2\phi^3 + p_3\phi^2 + p_4\phi + p_5 \quad (2.22)$$

$$[A]_x[p]_{x1} = [c_g]_{x2} + \text{error} \quad (2.23)$$

In these equations, $[p]$ is the coefficient vector (size 20×1), ϕ is the propagation direction, and $[c_g]$ is the group speed. The orientation ϕ is the connection matrix A (size 36×20), creating a formulation solved using a least-squares approach [Radhakrishna Rao and Toutenburg, 1999]. Extra interface conditions are applied such that every polynomial function is connected to the function of the next quarter. This is achieved by extending the rows of matrix A

$$[A]_{40,20} [p]_{n=1:20} = [c_g]_{m=1:40} + \text{error} \quad (2.24)$$

A fourth-order polynomial functions can describe up to three extrema. A third-order polynomial function has a maximum of two extreme values. The layout of the specimen is varied with 45° , this can result in three maximum group speeds per quarter, i.e., a maximum group speed every 45° . A fourth-order polynomial function is chosen to describe this effect.

It is possible to describe the group speed with higher-order polynomial functions. Higher-order polynomial functions may be better able to describe the measured values, and is recommended to be investigated in future research. The result of this is shown in section 4.3.

Error quantification

The model is 'optimized' if the difference between experimental and simulated group speeds is small, as described by Equation 2.25. The error is the distance between the measured group speed and the simulated group speed. The distance between these values is determined for every measured orientation in the plate.

$$\arg \min_{c_i \in C} \left(c_g^{m,exp}(f_i), c_g^{m,sim}(f_i) \right) < e \quad (2.25)$$

Sale et al. [2011] use a hybrid broadband laser/PZT ultrasonic set-up, elaborating more explicit on the optimization approach. The routine is based on the simplex search method [Nelder and Mead, 1965] solving the error function as described in Equation 2.26.

The error description is used in the optimization algorithm described in subsection 2.4.2.

$$\text{ERRf}(Mat, \rho) = \sum_{m=A_0, S_0} \left\{ \sum_{f_i} \left| \frac{c_g^{m,EXP}(f_i) - c_g^{m,SIM}(f_i)}{c_g^{m,SIM}(f_i)} \right|^2 \right\} \quad (2.26)$$

The summation of all the differences at every direction results in even weighting for every measurement. As is described in the previous section, the piecewise polynomial fit is applied on the experimentally determined group speeds.

2.4.2. Optimization Algorithm

An optimization algorithm is applied to minimize the quantified error using a least-squares approach. Two algorithms that are often used in characterization of FRC's are a direct search method and a genetic algorithm (GA).

Direct Search

Optimization using a direct search approach is a gradient based optimization method. This method is used for reconstruction of stiffness properties by Webersen et al. [2018] and Barazanchy et al. [2018]. An advantage of a direct search method is the use of less computational power. Finding a local minimum can be a challenge for direct search methods and circumvented by using a genetic algorithm.

Genetic Algorithm

A genetic algorithm is based on natural selection as is described by Darwin [Darwin, 1859]. The selection is based on a random starting population of which only the best performing combinations are preserved. These individuals are promoted to a next generation. These specimens are evolving slightly because of mutations of input parameters, or crossover between individuals. Five phases are considered in a genetic algorithm [Haupt and Haupt, 2004]:

1. Initial population (potential solutions)
2. Fitness function (to select potential solutions)
3. Selection (to preserve good solutions)
4. Crossover (jumps in solution space),
5. Mutation (to avoid stagnation)

The initial population is a random combination of parameters within the range that is given for every parameter. The bigger the population, the bigger the chance of a individual to be 'better' according the fitness function. A visual representation of both an elite child, crossover child and mutation child is shown in Figure 2.17 [Mathworks].

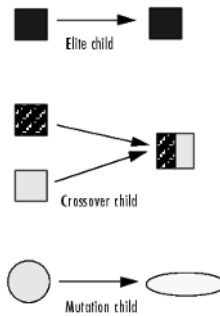


Figure 2.17: Children in a genetic algorithm

The initial population evolves as an evolutionary process. Every generation has the possibility to improve because of elitism, crossover, and mutation. Research by Kersemans et al. results in a combination between these possibilities as shown in Table 2.1.

Parameter	Value
Elite	0.2
Crossing	0.6
Mutation	0.2

Table 2.1: Settings for a genetic algorithm

The total required population and generations preferred in an optimization are researched. An overview is shown in Table 2.2. Both Ragauskas and Belevicius [2009], and Kersemans et al. [2014] propose a variable amount of generations, as long as the target accuracy is not yet met. Likewise research concludes a total of 100 generations and a population varying between 25 and 100 individuals is advised.

Research	Population	Generations
Ragauskas and Belevicius [2009]	40	
Marzani and De Marchi [2012]	50	100
Salmanpour et al. [2016]	100	100
Vishnuvardhan et al. [2007]	25	100
Kersemans et al. [2014]	100	

Table 2.2: Parameters for a genetic algorithm

An analysis of the minimum required amount of generations is shown in subsection 4.1.3. The conclusion from the analysis is that for the currently chosen application, a combination of 70 generations with a population of 70 is sufficient.

3

Experiments

The experiments that are conducted in order to retrieve the material properties of FRC-plates involve different components, settings and equipment. Each of them performs a crucial role in the retrieval of the ultrasonic guided waves propagating through the plate. The first part of this chapter will focus on the specifications of the test plates in section 3.1. This means the used material, layup and dimensions. What equipment is needed and what is the correct method of connecting them such that the signal is measured by the sensor is described in section 3.2. The exact settings, sensors, and sensor holders are described in subsection 3.3.2.

3.1. Plate Specifications

The description of the plate specifications is divided into the material, geometry and layup, and production process

Materials

The test plates are glass-fiber reinforced composites. The glass fiber used is produced by SearTex and is the unidirectional E-class fiber known as the $U - E - 640g/m^2$, as shown in Table 3.1. The volume percentage of this material is expected to be 48 %.

The resin is made by Atlec and is called E-Nova MA6215. This vinyl ester resin is especially created for offshore conditions and therefore ideal as a test material in an experiment that is supposed to be used in offshore conditions. The resin content is expected to be 52 %.

Material	Name	Vf [%]
Glass Fiber	SearTex $U - E - 640g/m^2$	48
Resin	Atlec E-Nova MA 6215	52
Hardener	Curox CM-75	-

Table 3.1: Material name

Name	Value	Unit
Fabric weights	600	g/m^2
Fiber density	2600	kg/m^3
Nr plies	18	-
Width	600	mm
Length	600	mm
Resin density	1200	kg/m^3
Fiber density	2600	kg/m^3
Overall density	1872	kg/m^3

Table 3.2: Material properties

Research about the influence of the fibers or fiber volume on the average weight and properties has been reported by SearTex [SearTex GmbH Co. KG, 2013].

Geometry and layup

The ply stacking sequence of the FRC samples are shown in Table 3.3. It shows the different layups of the model in addition to the expected thickness.

Specimen	1	2	3	4	5
Specification	0,90 symmetric balanced	0,45,-45,90 symmetric balanced	0,90,45 symmetric unbalanced	0,90 asymmetric balanced	0,90,45 asymmetric unbalanced
Fiber type	UD 600	UD 600	UD 600	UD 600	UD 600
Layer	Layup (°)	Layup (°)	Layup (°)	Layup (°)	Layup (°)
1	0	0	0	0	0
2	0	0	0	0	0
3	0	45	0	0	0
4	0	45	90	0	90
5	0	90	90	0	90
6	90	-45	90	90	90
7	90	90	45	90	45
8	90	90	45	90	45
9	90	90	45	90	45
10	90	90	45	90	0
11	90	-45	45	0	0
12	90	-45	45	0	0
13	90	45	09	0	90
14	90	45	90	0	90
15	90	0	90	0	90
16	0	0	0	90	45
17	0		0	90	45
18	0		0	90	45
19	0			90	
20	0			90	
Total thickness	10.2 mm	8.16 mm	9.18 mm	10.2 mm	9.18 mm

Table 3.3: Ply stacking sequence

A visual representation of these specimen is shown in Figure 3.1. It shows there is a variation of symmetrical opposed to asymmetrical layups, with a combination of balanced and unbalanced layups.

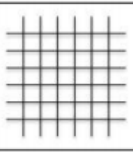
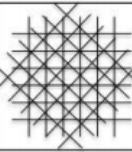
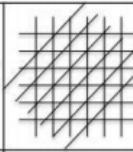
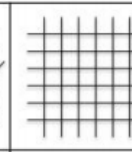
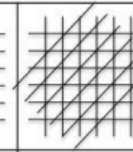
	Specimen 1	Specimen 2	Specimen 3	Specimen 4	Specimen 5
					
Plies orientation	0, 90	0, 45, -45, 90	0, 90, 45	0, 90	0, 90, 45
Lamination	Symmetric, balanced	Symmetric, balanced	Symmetric, unbalanced	Asymmetric, balanced	Asymmetric, unbalanced
Dimensions mm x mm x mm	600x600x10	600x600x10	600x600x10	600x600x10	600x600x10

Figure 3.1: Layups

Production Processes

The process of production of these composite plates is performed by using vacuum infusion. The layup is placed by hand instead of with a spray gun or with a filament winding. This is to create the specific layup that is preferred during the experiments.

The process of vacuum infusion starts with the prepared vinylester resin. This resin is pumped through the resin inlet to the mold by a vacuum pump. The resin propagates through the mold towards the vacuum outlet and resin trap. The flow of the resin through the mold is visible in Figure 3.2. The resin will not spread evenly if the plate is too large, i.e., the flow path is too large. A flow path between the plates ensures even distribution. The flow path is the dark line between the plates on the left, and the plates on the right in Figure 3.2a.

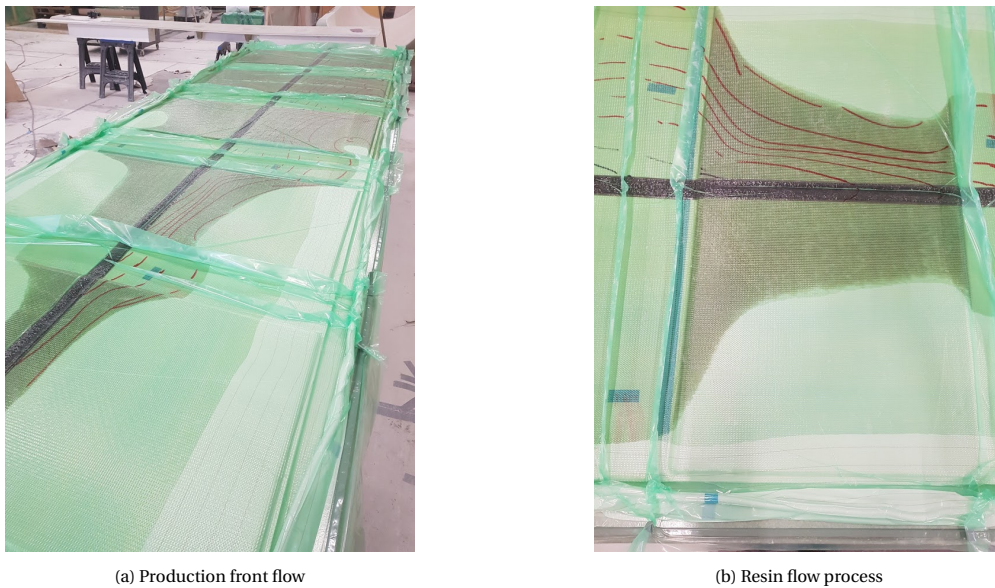


Figure 3.2: Production of the plates

A representation of the resin flow process is shown in Figure 3.3. The flow paths ensure that the distance the resin has to travel through the mold is no more than the width of the plate [composites.ugent.be, 2020].

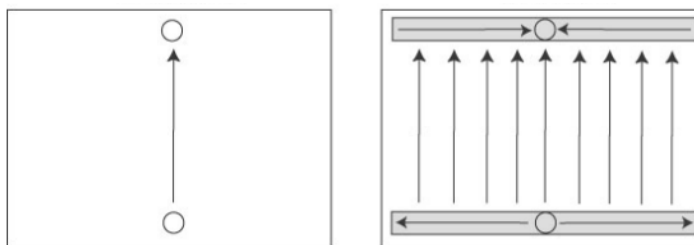


Figure 3.3: Flow of resin

The total needed amount of resin is prepared on the input side of the mold as shown in Figure 3.4a. The filled path of resin in between the plates and the infused plates are shown in Figure 3.4b.



(a) Production Resin



(b) Production Center Line

Figure 3.4: Resin used in production the plates

3.2. Experiment setup

The architecture of the measurement system is described next. An illustration of the architecture is shown in Figure 3.5. The process is branched in a guided wave generating side, and a receiving side.

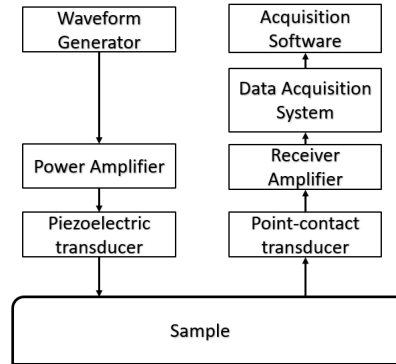


Figure 3.5: Measurement system

Waveform Generator

The start of the setup is in this experiment the waveform generator that is shown in Figure 3.6. The waveform generator has the function to create it's own wave signal, or produce a pre-loaded waveform. The pre-loaded waveform that will be used is described in section 3.3. The mathematics of creating this wave signal is described in subsection 2.2.1

High Voltage Amplifier

The waveform generator is connected to the high voltage amplifier. This amplifier is shown in Figure 3.7. This amplifier has a voltage gain of 50 times the input value. This means that the 10 V that was created in the waveform generator is amplified to 500 V before it is connected to the actuator.



Figure 3.6: Waveform generator

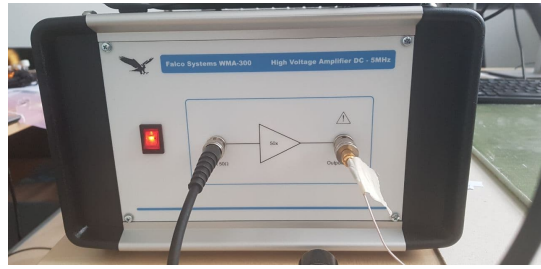


Figure 3.7: High voltage amplifier

Vallen Actuator

A conventional piezoelectric transducer with a flat surface has been used as the actuator. This transducer was placed in the middle of the plate and was not moved during the experiment. The transducer type was VS600-Z1, shown in Figure 3.8. This transducer shows a resonance at around 600 kHz.



Figure 3.8: Vallen transducer

Pre-amplifier

The voltage created by the sensor is transmitted through a cable to a pre-amplifier. This passive amplifier is shown in Figure 3.9. The model used in this experiment is the 'AEP5H' model. The pre-amplifier and the Data Acquisition System (DAS) are both designed by Vallen [Vallen System, 2020b].



Figure 3.9: Pre-amplifiers

A voltage amplification of 40 dB is created as is shown in Figure 3.10. The blue dotted line shows an optimal range between 100 kHz and 1 MHz. The amplification decreases at lower frequencies.

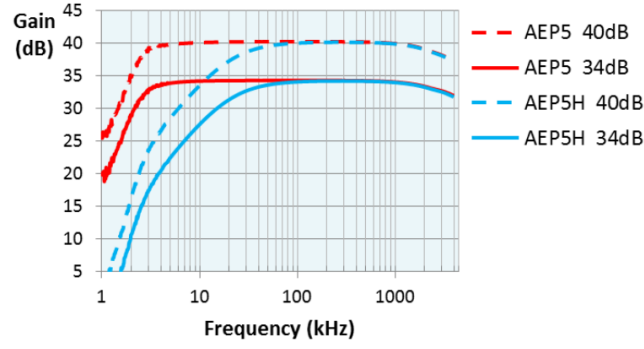


Figure 3.10: Frequency response

The amplification of the signal is 40 dB as discussed. This is shown in Equation 3.1 and Equation 3.2. The power of 2 and the multiplication in Equation 3.2 is custom because the amplification of power is subject to voltage squared. The amplification of 40 dB is equivalent to a voltage gain of 100. Which is beneficial to the data acquisition system.

$$N_{dB} = 10 \log_{10} \left(\frac{V_{out}^2}{V_{in}^2} \right) \quad (3.1)$$

$$N_{dB} = 20 \log_{10} \left(\frac{V_{out}}{V_{in}} \right) \quad (3.2)$$

Data Acquisition System

The amplified signal is loaded into the Data Acquisition System (DAS) by Vallen, shown in Figure 3.11. The chassis is the MB6 type as is described in "AMSY-6 System Specification" [Vallen System, 2020a]. The system is able to both measure the amount of Accoustic Emissions (AE) and Transient Recordings (TR)



Figure 3.11: Data acquisition system

The sample rate (f_s) of the DAS is determined based on the preferred maximum frequency of the guided waves (B). In short, the minimal sample rate is required to be double that of the wave frequency in order to prevent aliasing. Passing this Nyquist frequency can cause problems when transposing the measured signal between domains, creating artifacts that did not exist in the original signal. As the preferred frequency of the guided waves is below 100 kHz, it means that the measuring frequency of the DAS is sufficient to detect voltage fluctuations transmitted by the pre-amplifier [Amidror, 2015]. Having a DAS that is able to measure at up to 10 MHz results in a maximum capability of measuring guided waves with a frequency of 5 MHz. This is known as the Nyquist frequency. The minimum sampling rate (f_s) is thus

$$f_s > 2B. \quad (3.3)$$

Where B is the existing frequency.

The DAS measures a transient signal based on passing a threshold amplitude. This makes it possible to only save the relevant transient recordings. Oversampling will therefore not be a problem and a highest possible sampling rate is preferred in the experiments.

The next chapter will describe the steps and processes that have to do with acquiring the preferred signals and data.

3.3. Point contact transducer

The receiving transducer used in the experiments is dry-point-contact(DPT) transducer by ACS. This transducer has a nominal frequency of 100 KHz and is applied for excitation or acquiring ultrasonic waves.

The tip of the point contact piezoelectric transducer is shown in Figure 3.12.

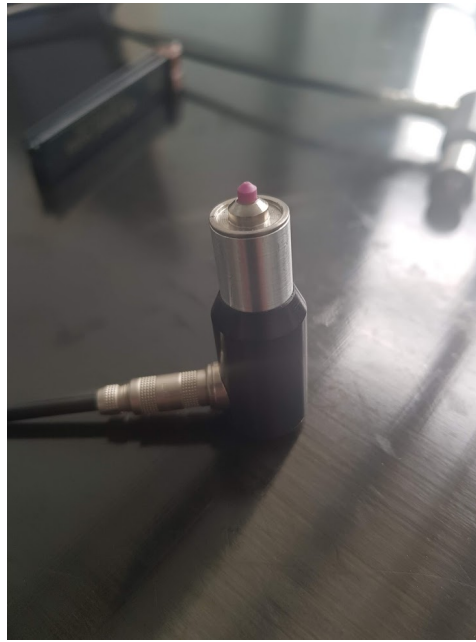


Figure 3.12: Cone closeup

3.3.1. Sensor holder

Crucial in these type of experiments is that the conditions of the test should remain as constant as possible. One of the most important factors is the distance between sensors, such that the group speed between them can be determined. In order to achieve constant distance between sensors, a sensor holder has been designed. This sensor holder has other advantages. The first of which is that it creates the possibility to place the sensors on the structure robustly without having to hold them by hand. The additional benefit is that the amplitude of the signal is constant as the pressure with whom the sensor is connected to the substructure is constant.

The sensor holder can be supported at the ends to ensure that the point contact transducers are orthogonal to the surface of the plate. This also created the possibility to add weight on top of the construction. This weight is divided in pressure across the structure as the screws are only in contact with the acrylic plate. The next figures show the eventual construction. Figure 3.13 shows the complete setup with 3 of the 4 places used by a sensor. Figure 3.14 shown a detail of an individual point contact transducer. The pressure by which the sensor is pressed onto the surface is applied by the rubber band between the upper acrylic plate and the sensor. The lower acrylic plate has a hole with a smaller diameter to prevent the sensor from dropping out, and to keep the sensor exactly vertical



Figure 3.13: Sensor holder

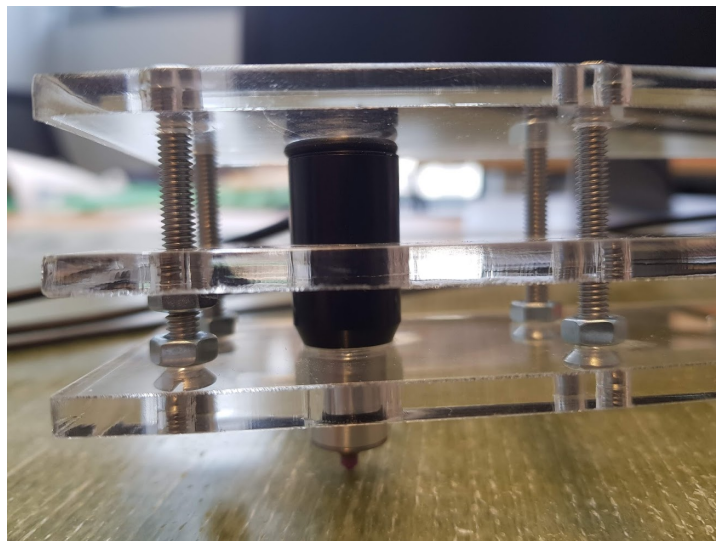


Figure 3.14: Close up of sensor holder

3.3.2. Settings and Reflecting Waves

Factors influencing the choices with respect to the design are among others the expected dispersion curves. The dimensions of the plate make the possibility for a fixed actuator in the center without the need for a movement of the actuator. Which can create more variations to the signals.

The final design and orientations of the point contact transducers is shown in Figure 3.15. This is a top view of the locations of all the sensors. The distance between all sensors is fixed to 60 mm using the sensor holder. The steps with respect to direction are kept constant at 10 degrees across the entire circle.

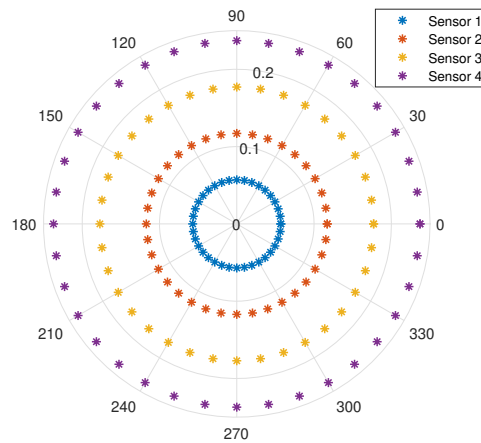


Figure 3.15: Sensor Setup

A picture of this same setup is shown in Figure 3.16. The cables connecting the sensors to the amplifiers are shown as well, including the numbered amplifiers.

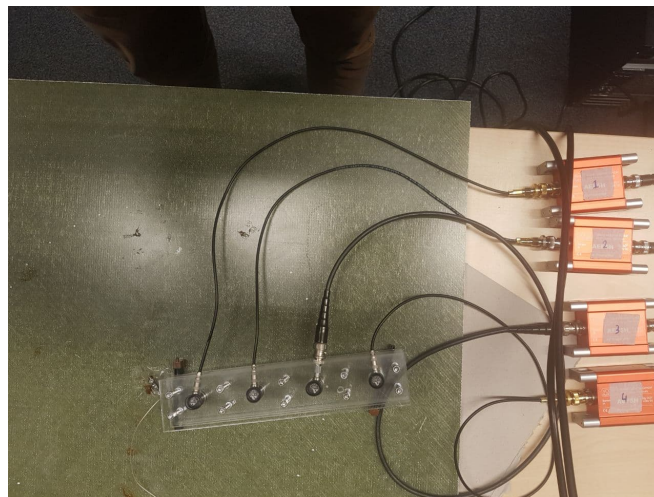


Figure 3.16: Conic sensor on plate

The waveform created using the waveform generator, as described in in Table 3.4, has a maximum voltage per peak of 10 volt. This voltage per peak is created as described in subsection 2.2.1. The center frequency of the wave that was prepared is 60 kHz. In order to average the signal to improve the measured signal, every orientation has been measured for a minimum 32 times. This was done during a minimum of 32 seconds as the period between every burst is 1.00 second.

Nr of Pulses	5	-
Voltage	10	V_{pp}
Center frequency	60	kHz
Burst period	1.00	s
Total bursts	32	-

Table 3.4: Waveform Generator Settings

The settings used in the DAS are shown in Table 3.5. The pre-trigger value of $200 \mu s$ is chosen. This creates a number of advantages. Firstly, it creates the possibility to window the relevant piece of the signal. Secondly, a pre-trigger enables the option to asses the buildup in the signal before the trigger time for quality control of the recordings.

Pre-trigger	200	μs
Sampling rate	10	MHz
Rearm time	250	μs
Signal length	812.9	μs
Threshold value	30.1	dB

Table 3.5: Data Acquisition Settings

4

Results and Discussion

This Chapter shows the results of application of the method described in Chapter 2 in the experimental setup described in chapter 3. First, an analysis of the sensitivity of the material properties will be studied regarding the effect of a change in properties on group speed of each wave mode. Secondly, the method as described in Chapter 2 will be deployed on simulated data. This will be shown in Chapter 4.2.

Finally, the measured data is analyzed and used for estimation of the material properties. The data is coming from the setup as is described in 3.

4.1. Sensitivity Analysis

The sensitivity analysis focuses on the effect of changes in the material properties on the dispersion curve first. Next, the effect from production errors is discussed. Section 4.1.3 describes the accuracy of the minimization algorithm based on exact input values.

4.1.1. Effect of Changing Material Properties

The effect of a change in material properties on the dispersion speed is investigated before optimizing for this dispersion speed. The material properties of an example plate are varied with 30 % in both directions. The analysis will focus of frequencies between 50 kHz and 200 kHz. This is a range of frequencies for which the least amount of higher order dispersive waves are present. The material properties used in the analysis are shown in Table 4.1. The orientation of the fibers is show in Figure 4.1. The change in percentage is based on the group speed of both modes as determined with the described material properties.

Property	Symbol	Value	Unit
Young's Modulus	E_{11}	46.2	Gpa
Young's Modulus	E_{22}, E_{33}	13.1	Gpa
Shear Modulus	G_{12}, G_{13}	4.1	Gpa
Shear Modulus	G_{23}	5.1	Gpa
Poisson's Ratio	ν_{12}, ν_{13}	0.29	-
Poisson's Ratio	ν_{23}	0.28	-
Additional Property's	Symbol	Value	Unit
Density	ρ	1872	kg/m^3
Thickness	t	9.2	mm
Layup	θ	$[0]_{12}$	$^\circ$

Table 4.1: Material Properties

The first material property is the Young's Modulus in the longitudinal direction. Varying this parameter has a large influence on the dispersion speed of the S_0 -wave at all frequencies. A variation of 30 % of the Young's modulus results in anywhere between 10 % and 20 % in the same direction. Higher frequencies of the guided wave show an opposite effect.

The dispersion speed of guided waves propagating in direction '2' are barely influenced by variations of the E_1

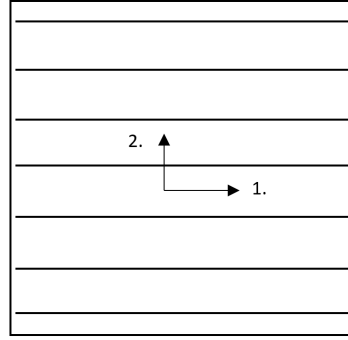


Figure 4.1: Fiber direction

value. This is as expected as fibers in one direction do not influence either the strength nor the speed of transmission of the energy of a wave in the other direction.

Effects described in the previous paragraph are similar when looking at a 90° direction. Difference is that the change in speed is higher. A change in the Young's Modulus (E_{22} E_{33}) of 30 % can vary the propagation speed with more than 40 % when looking at a frequency of 150 kHz.

The propagation speed of the guided waves in the fiber direction decreases when the shear modulus (G_{12} , G_{13}) is decreased, and can be increased the other way around. It is remarked that the change in speed is nearly constant over the range of different frequencies. Similar effects are seen in propagation speeds perpendicular to the fiber direction when G_{23} is varied.

The effect of the density (of the combined resin and fiber) is relatively constant with respect to the anti-symmetric wave (A_0). The speed increases with roughly 20 % when the density of the plate is reduced with 30 percent. Increasing the density of the plate with 30 % results in roughly 20 % increase at lower frequencies. This is in line with expectations. The increase in mass is correlated with speed propagation (c) as is shown in Equation 4.1 for a 1D analogy.

$$c = \sqrt{\frac{K}{M}} \quad (4.1)$$

With K and M the stiffness and mass respectively. Roughly the same effect can be observed when looking at the symmetric wave (S_0). However, the effect of the density of the material increases with higher frequencies reaching 60 % decrease in speed when the density is increased with 30 %. A reduction of the density results in an increase in propagation speed of as much as 90 % at 150 kHz and perpendicular to the fiber direction, as can be seen in Table 4.4. The propagation speed of 200 kHz moves back to original values. This is because, after a decrease in propagation speed for increasing frequencies, the propagation speed of the symmetrical wave starts to increase again. The amount by which this increase has already started at 200 kHz mostly effects the change in density has on the propagation speed at this specific frequency.

The propagation of the antisymmetric wave is barely influenced by changes in thickness of the plate. The difference in speed is barely more than 0.5 % for a change of 30 percent. This half a percent is reached when the frequency of the waves is in the higher range of tested frequencies. The propagation speed of the symmetric wave increases with lower thicknesses of the material. This effect can be observed in both directions of the fibers in the material. A sharp increase in propagation speed can be observed at 200 kHz and an increased thickness of the plate.

Frequency Unit	50 [kHz] Cg (m/s)/%	100 [kHz] Cg (m/s)/%	150 [kHz] Cg (m/s)/%	200 [kHz] Cg (m/s)/%	Wave Type
$0.7 \cdot E_1$	1.4746 (100.1)	1.4772 (100.0)	1.4761 (100.2)	1.4712 (100.3)	A_0
	3.5329 (84.0)	3.2234 (81.9)	1.7458 (81.1)	1.012 (108.0)	S_0
$0.7 \cdot E_2, E_3$	1.4710 (99.8)	1.4753 (99.9)	1.4733 (100.0)	1.4674 (100.0)	A_0
	4.1739 (99.3)	3.7501 (95.3)	0.7795 (36.2)	1.1096 (118.3)	S_0
$0.7 \cdot G_{12}, 0.7 \cdot G_{13}$	1.2353 (83.8)	1.2340 (83.5)	1.2259 (83.2)	1.2197 (83.1)	A_0
	4.2029 (100.0)	3.9267 (99.8)	2.1274 (98.8)	0.7405 (79.0)	S_0
$0.7 \cdot G_{23}$	1.4738 (100.0)	1.4772 (100.0)	1.4737 (100.0)	1.4672 (100.0)	A_0
	4.2029 (100.0)	3.9268 (99.8)	2.1578 (100.3)	0.9374 (100.0)	S_0
$0.7 \cdot \nu_{12}, 0.7 \cdot \nu_{13}$	1.4696 (99.7)	1.4753 (99.9)	1.4736 (100.0)	1.4678 (100.0)	A_0
	4.1815 (99.5)	4.0391 (102.6)	2.6237 (121.9)	0.9160 (97.7)	S_0
$0.7 \cdot \nu_{23}$	1.4726 (99.9)	1.4766 (100.0)	1.4735 (100.0)	1.4672 (100.0)	A_0
	4.2077 (100.1)	3.9469 (100.3)	1.9618 (91.2)	0.9554 (101.9)	S_0
Density $0.7 \cdot [\rho]$	1.7607 (119.5)	1.7648 (119.5)	1.7645 (119.7)	1.7587 (119.9)	A_0
	5.0431 (120.0)	4.8622 (123.5)	4.1045 (190.7)	1.2586 (134.2)	S_0
Thickness $0.7 \cdot [d]$	1.4712 (99.8)	1.4753 (99.9)	1.4772 (100.2)	1.4748 (100.5)	A_0
	4.2301 (100.6)	4.1399 (105.2)	3.8647 (179.6)	2.8165 (300.5)	S_0
Original	1.4734 (100.0)	1.4771 (100.0)	1.4736 (100.0)	1.4671 (100.0)	A_0
	4.2043 (100.0)	3.9363 (100.0)	2.1522 (100.0)	0.9376 (100.0)	S_0

Table 4.2: Dispersion speed along fiber direction with material parameters at $\cdot 70\%$

Frequency Unit	50 [kHz] Cg (m/s)/%	100 [kHz] Cg (m/s)/%	150 [kHz] Cg (m/s)/%	200 [kHz] Cg (m/s)/%	Wave Type
$1.3 \cdot E_1$	1.4732 (100.0)	1.4769 (100.0)	1.4712 (99.8)	1.4639 (99.8)	A_0
	4.7813 (113.7)	4.5349 (115.2)	2.6009 (120.8)	0.8948 (95.4)	S_0
$1.3 \cdot E_2, 1.3 \cdot E_3$	1.4757 (100.2)	1.4785 (100.1)	1.4739 (100.0)	1.4669 (100.0)	A_0
	4.2320 (100.7)	4.0059 (101.8)	3.0628 (142.3)	0.9636 (102.8)	S_0
$1.3 \cdot G_{12}, 1.3 \cdot G_{13}$	1.6779 (113.9)	1.6811 (113.8)	1.6826 (114.2)	1.6792 (114.5)	A_0
	4.2029 (100.0)	3.9268 (99.8)	2.1765 (101.1)	1.1074 (118.1)	S_0
$1.3 \cdot G_{23}$	1.4738 (100.0)	1.4772 (100.0)	1.4737 (100.0)	1.4672 (100.0)	A_0
	4.2029 (100.0)	3.9268 (99.8)	2.1578 (100.3)	0.9374 (100.0)	S_0
$1.3 \cdot \nu_{12}, 1.3 \cdot \nu_{13}$	1.4788 (100.4)	1.4795 (100.2)	1.4734 (100)	1.4662 (99.9)	A_0
	4.2313 (100.6)	3.7842 (96.1)	1.8592 (86.4)	0.9650 (99.9)	S_0
$1.3 \cdot \nu_{23}$	1.4751 (100.1)	1.4780 (100.1)	1.4742 (100.0)	1.4670 (100.0)	A_0
	4.1967 (99.9)	3.9054 (99.2)	2.3491 (109.1)	0.9216 (98.3)	S_0
Density $1.3 \cdot [\rho]$	1.2929 (87.8)	1.2954 (87.7)	1.2901 (87.6)	1.2838 (87.5)	A_0
	3.6704 (87.3)	3.2603 (82.8)	0.8333 (38.7)	0.9304 (99.2)	S_0
Thickness $0.7 \cdot [d]$	1.4748 (100.1)	1.4759 (99.9)	1.4678 (99.6)	1.4604 (99.5)	A_0
	4.1593 (98.9)	3.2792 (83.3)	0.9128 (42.4)	1.1562 (123.3)	S_0
Original	1.4734 (100.0)	1.4771 (100.0)	1.4736 (100.0)	1.4671 (100.0)	A_0
	4.2043 (100.0)	3.9363 (100.0)	2.1522 (100.0)	0.9376 (100.0)	S_0

Table 4.3: Dispersion speed along fiber direction with material parameters at $\cdot 130\%$

Frequency Unit	50 [kHz] Cg (m/s)/%	100 [kHz] Cg (m/s)/%	150 [kHz] Cg (m/s)/%	200 [kHz] Cg (m/s)/%	Wave Type
$0.7 \cdot E_1$	1.1846 (100.1)	1.1856 (100.0)	1.1801 (100.0)	1.1740(100.0)	A_0
	2.9755 (100.7)	2.6675 (99.8)	1.4337 (101.4)	0.8137(100.2)	S_0
$0.7 \cdot E_2, 0.7 \cdot E_3$	1.1807 (99.8)	1.1832 (99.8)	1.1823 (100.2)	1.1783(100.3)	A_0
	2.4383 (82.5)	1.9959 (74.7)	0.8333(59.0)	0.9454(116.4)	S_0
$0.7 \cdot G_{12}, 0.7 \cdot G_{13}$	1.1834 (100.0)	1.1852 (100.0)	1.1803 (100.0)	1.1744(100.0)	A_0
	2.9542 (100.0)	2.6733 (100.0)	1.4135 (100.0)	0.8121(100.0)	S_0
$0.7 \cdot G_{23}$	0.9920(83.8)	0.9883(83.4)	0.9811(83.1)	0.9765(83.1)	A_0
	2.9542 (100.0)	2.6727 (100.0)	1.3399 (94.8)	0.6346(78.1)	S_0
$0.7 \cdot \nu_{12}, 0.7 \cdot \nu_{13}$	1.1820 (99.9)	1.1847 (100.0)	1.1805 (100.0)	1.1748(100.0)	A_0
	2.9291 (99.2)	2.6796 (100.2)	1.3868 (98.1)	0.8118(100.0)	S_0
$0.7 \cdot \nu_{23}$	1.1798 (99.7)	1.1838 (99.9)	1.1803 (100.0)	1.1748(100.0)	A_0
	2.9779 (100.8)	2.8092 (105.1)	1.6125 (114.1)	0.7853(96.7)	S_0
Density $0.7 \cdot [\rho]$	1.4136 (119.5)	1.4169 (119.5)	1.4141 (119.8)	1.4082(119.9)	A_0
	3.5518 (120.2)	3.3637 (125.8)	2.6684 (188.8)	1.1026(135.8)	S_0
Thickness $0.7 \cdot [d]$	1.1814 (99.8)	1.1849 (100.0)	1.1849 (100.4)	1.1815(100.6)	A_0
	2.9830 (101.0)	2.8882 (108.0)	2.6134 (184.9)	1.7860(219.9)	S_0
Original	1.1835 (100.0)	1.1852 (100.0)	1.1801 (100.0)	1.1743(100.0)	A_0
	2.9541 (100.0)	2.6733 (100.0)	1.4132 (100.0)	0.8122(100.0)	S_0

Table 4.4: Dispersion speed perpendicular to the fiber direction with material parameters at $\cdot 70\%$

Frequency Unit	50[kHz] Cg (m/s)/%	100 [kHz] Cg (m/s)/%	150 [kHz] Cg (m/s)/%	200 [kHz] Cg (m/s)/%	Wave Type
$1.3 \cdot E_1$	1.1828 (99.9)	1.1849 (100.0)	1.1804 (100.0)	1.1746(100.0)	A_0
	2.9428(99.6)	2.6763 (100.1)	1.4018 (99.2)	0.8118(100.0)	S_0
$1.3 \cdot E_2, 0.7 \cdot E_3$	1.1851 (100.1)	1.1847 (100.0)	1.1774 (99.8)	1.1712(99.7)	A_0
	3.4021 (115.2)	3.1785 (118.9)	2.3299 (164.8)	0.8054(99.2)	S_0
$1.3 \cdot G_{12}, 1.3 \cdot G_{13}$	1.1834 (100.0)	1.1852 (100.0)	1.1803 (100.0)	1.1744(100.0)	A_0
	2.9542 (100.0)	2.6733 (100.0)	1.4135 (100.0)	0.8121(100.0)	S_0
$1.3 \cdot G_{23}$	1.3472 (113.8)	1.3502 (113.9)	1.3495 (114.3)	1.3451(114.5)	A_0
	2.9542 (100.0)	2.6737 (100.0)	1.4616 (103.4)	0.9703(119.5)	S_0
$1.3 \cdot \nu_{12}, 1.3 \cdot \nu_{13}$	1.1854 (100.2)	1.1859 (100.1)	1.1800 (100.0)	1.1738(100.0)	A_0
	2.9886 (101.2)	2.6637 (99.6)	1.4452 (102.2)	0.8153(100.4)	S_0
$1.3 \cdot \nu_{23}$	1.1877 (100.4)	1.1868 (100.1)	1.1803 (100.0)	1.1739(100.0)	A_0
	2.9243 (99.0)	2.5268 (94.5)	1.3067 (92.4)	0.8392(103.3)	S_0
Density $1.3 \cdot [\rho]$	1.0384 (87.7)	1.0387 (87.6)	1.0329 (87.5)	1.0276(87.5)	A_0
	2.5745 (87.1)	2.1718 (81.2)	0.7636 (54.0)	0.7709(94.9)	S_0
Thickness $1.3 \cdot [d]$	1.1845 (100.1)	1.1827 (99.8)	1.1749 (99.5)	1.1691(99.5)	A_0
	2.9085 (99.8)	2.1102 (78.9)	0.8029 (56.8)	0.9424(116.0)	S_0
Original	1.1835 (100.0)	1.1852 (100.0)	1.1801 (100.0)	1.1743(100.0)	A_0
	2.9541 (100.0)	2.6733 (100.0)	1.4132 (100.0)	0.8122(100.0)	S_0

Table 4.5: Dispersion speed perpendicular to the fiber direction with material parameters at $\cdot 130\%$

4.1.2. Effect from Production Errors

Non-destructive testing using piezoelectric transducers is applied in literature to measure production errors or damage localization. However, the current system has not yet achieved an accuracy in data acquisition nor data analysis, that small damages can be detected. Future research is required to incorporate the analysis of production errors in the estimation of material properties.

4.1.3. Accuracy of the Minimization Algorithm

The final step in the estimation of material properties is the matching error minimization process as described in subsection 2.4.2. This information is applied and tested on the current experiment on plate 1. Different combinations of settings of the genetic algorithm are tested such that the accuracy of the genetic algorithm can be assessed. The combinations of population and total amount of generations is varied from 10 to 150. The input of the algorithm in this section is the exact group speed that is determined by the same semi-analytical method as is used in the genetic algorithm itself. The only error that is created by this method is therefore the genetic algorithm itself.

The function score of this analysis is shown in Table 4.6. The function score of the different combinations of settings range from 0.159 to $5.7 \cdot 10^{-6}$. An decrease in the function score, and thus an increase in the estimation is achieved with higher populations, and more generations. The best score is however not achieved in the lower right part of the figure. The best score is found with a population of 100 and 40 generations.

A value of 0 is the optimum score, as there is no difference between the input data and the group speeds based on the estimation from the genetic algorithm. There are 36 orientations at which the group speed is determined, both for the symmetric and the anti-symmetric guided waves. Defining the average difference between the algorithm estimation and the input can be done by dividing the function score by the 72 different data points that are thus determined. The best score of $5.739 \cdot 10^{-6}$ results in an average score per direction of 0.028 %. Potential data points which deviate more can move this score disproportionately because of the square root in the fitness function. The score of $1.2162 \cdot 10^{-3}$ is equal to an average error of 0.411 %.

		Generations					
Population		10	20	40	70	100	150
	10	159.7402	49.3023	15.0346	7.0822	2.1969	11.4503
	20	9.1118	4.0181	4.7489	3.2038	0.0625	0.1038
	40	2.9981	0.1622	1.2162	0.3088	1.0395	1.6241
	70	18.9476	0.2966	0.3128	0.0237	0.2121	0.0353
	100	0.1831	0.5841	0.0057	0.1006	0.1017	0.0417
	150	0.1162	0.3246	0.0135	0.1063	0.0154	0.1576

Table 4.6: Function score · 1000

The material properties that belong to the function scores are shown in Table 4.7 to Table 4.11. The difference in results in the lower right of the table is within 10 % of the Young's modulus and the Shear modulus that was applied as an input value. The Poisson's ratio differs more, ranging from 0.2262 to 0.4079 [-].

		Generations					
Population		10	20	40	70	100	150
	10	35.1984	37.1636	41.5545	45.4282	43.3955	41.3744
	20	49.2632	43.5152	44.4977	42.7386	46.6832	45.6739
	40	47.2459	46.9805	47.4540	47.2699	47.9730	43.5557
	70	40.1158	45.2307	47.2329	45.8545	45.1519	46.5700
	100	45.3180	44.3646	46.1331	46.8205	45.5022	45.7620
	150	46.3578	44.8625	45.9584	45.4982	46.4462	44.8000

Table 4.7: Estimation of Young's modulus E1

		Generations					
Population		10	20	40	70	100	150
	10	15.9092	18.0472	17.3430	14.3595	15.9537	17.1877
	20	11.5323	15.5635	13.1564	16.0211	12.6707	13.7952
	40	12.8237	12.2534	12.0032	12.0418	11.7904	15.8017
	70	16.7088	14.3764	12.0182	13.4618	14.2916	12.6753
	100	14.1847	15.1869	13.2057	12.4042	13.9061	13.6058
	150	13.2221	14.5795	13.3797	13.9239	12.8177	14.6943

Table 4.8: Estimation of Young's modulus E2 & E3

		Generations					
Population		10	20	40	70	100	150
	10	0.4216	0.4035	0.4497	0.3732	0.4500	0.4444
	20	0.2094	0.3988	0.2602	0.4460	0.2524	0.3417
	40	0.2852	0.2122	0.2365	0.2043	0.2006	0.4500
	70	0.4422	0.3904	0.2061	0.3081	0.3761	0.2468
	100	0.3672	0.4434	0.2901	0.2262	0.3433	0.3197
	150	0.2948	0.3898	0.3025	0.3462	0.2574	0.4079

Table 4.9: Estimation of Poisson's ratio ν_{23}

		Generations					
Population		10	20	40	70	100	150
	10	4.0177	2.8568	3.0669	3.6726	3.5668	3.2070
	20	4.6878	3.5054	3.9990	3.5782	4.1930	3.9978
	40	4.0799	4.2529	4.3973	4.3282	4.3997	3.5960
	70	3.5027	3.9069	4.3274	4.0394	3.9119	4.1777
	100	3.9284	3.7726	4.0816	4.2276	3.9682	4.0133
	150	4.0798	3.8491	4.0526	3.9667	4.1499	3.8495

Table 4.10: Estimation of the Shear modulus G_{12}, G_{13}

		Generations					
Population		10	20	40	70	100	150
	10	4.0177	2.8568	3.0669	3.6726	3.5668	3.2070
	20	4.6878	3.5054	3.9990	3.5782	4.1930	3.9978
	40	4.0799	4.2529	4.3973	4.3282	4.3997	3.5960
	70	3.5027	3.9069	4.3274	4.0394	3.9119	4.1777
	100	3.9284	3.7726	4.0816	4.2276	3.9682	4.0133
	150	4.0798	3.8491	4.0526	3.9667	4.1499	3.8495

Table 4.11: Estimation of the Shear modulus G_{23}

The mean and the standard deviation of the results from the lower right of the table in shown in Table 4.12.

Property	Unit	Symbol	Input	Mean	Std	COV (%)
Young's Modulus	Gpa	E_{11}	46.2	45.8228	0.6756	1.47
Young's Modulus	Gpa	E_{22}, E_{33}	13.1	13.5312	0.7704	5.69
Shear Modulus	Gpa	G_{12}, G_{13}	4.1	4.0338	0.1274	3.16
Shear Modulus	Gpa	G_{23}	5.1	5.1441	0.0538	0.61
Poisson's Ratio	-	ν_{12}, ν_{13}	0.29			
Poisson's Ratio	-	ν_{23}	0.28	0.3146	0.0613	19.49
Additional Property's	Unit	Symbol	Value			
Density	kg/m^3	ρ	1872			
Thickness	mm	t	9.2			

Table 4.12: Material estimations of iterations with longest optimization

4.2. Results for Simulated Signals

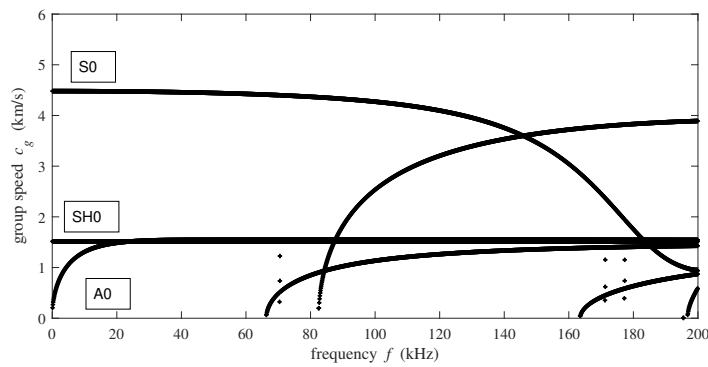
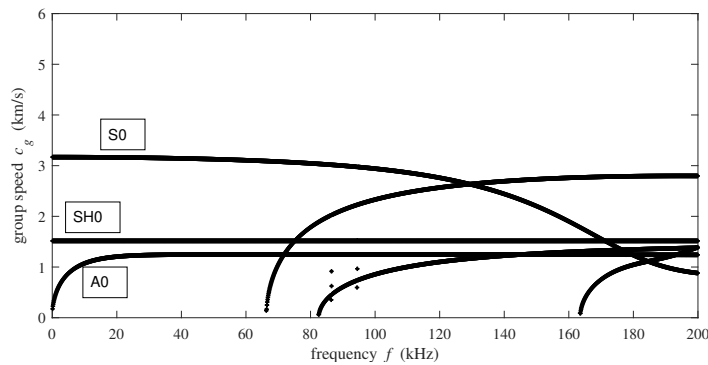
This section will show the results of material property estimation with the use of simulated signals. This means that both the signals from the actuator and the sensors are simulated. The used material properties used for the material property estimation are shown in Table 4.13.

Property	Symbol	Value	Unit
Young's Modulus	E_{11}	35.0	Gpa
Young's Modulus	E_{22}, E_{33}	17.5	Gpa
Shear Modulus	G_{12}, G_{13}	4.18	Gpa
Shear Modulus	G_{23}	2.7	Gpa
Poisson's Ratio	ν_{12}, ν_{13}	0.29	-
Poisson's Ratio	ν_{23}	0.28	-
Additional Property's	Symbol	Value	Unit
Density	ρ	2020	kg/m^3
Thickness	t	0.97	cm

Table 4.13: Material properties in the numerical simulation

Dispersion Curve

The dispersion speed is dependent on the material properties, layup, and thickness of the laminate. The effect of the directions of the fibers is shown in Figure 4.2 and Figure 4.3. Based on the modes shapes, it is possible to describe which of these curves is the A_0 wave and which is the S_0 wave.

Figure 4.2: Dispersion Curve at 0° Figure 4.3: Dispersion Curve at 90°

A couple of remarks can be made based on these figures and the discussion in subsection 2.1.1. The first one is that the propagation speed of S_0 waves is higher in the direction of the fibers. This is as expected since S_0 is dominated by the longitudinal stiffness of the laminate. The second comment is that there is a low amount of dispersion in the frequency spectrum between 20 kHz and 100 kHz. Therefore, measurements of multiple frequencies in this range would provide limited additional information. In the remainder of this chapter, the analysis is limited to a center frequency of 60 kHz. Selection of the propagation speed at 60 kHz is displayed in Figure 4.4. The dispersion curve is sorted as described in chapter 2. The A_0 and S_0 modes can be identified at 0 kHz. And are identified when reaching higher frequencies. This is shown for a plate with material properties according to Table 4.13 and a laminate layup of $[90]_{12}$.

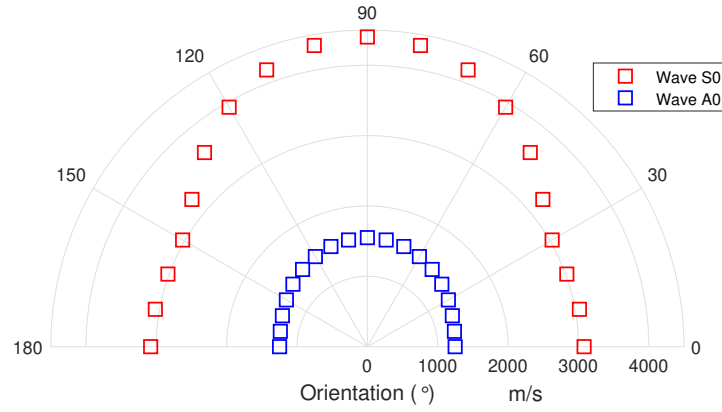


Figure 4.4: Dispersion Speed at 60 kHz

Simulate Signal

The next step is to simulate both the source signal and the measured signal for similar layups used in the experiment. The method on which this is based is described in subsection 2.2.1. The actuator signal consists of 5-cycle Hanning windowed sinusoidal waves with a center frequency of 60 kHz. The centre frequency of the signal is visible in the lower part of Figure 4.5.

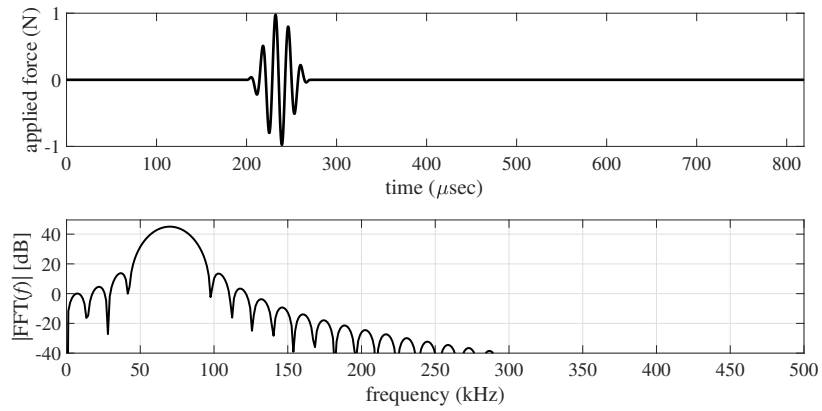


Figure 4.5: Source Signal

The actuator signal is simulated at the location of the sensor as is shown in Figure 4.6. The process that is used to achieve this simulated dispersed signal is described in subsection 2.2.4. The methodology of extraction of arrival times was given in section 2.3.

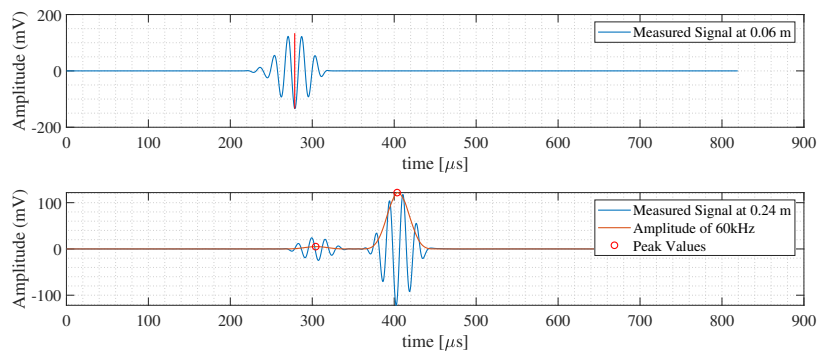


Figure 4.6: Simulated signal from sensors

The difference in amplitude of the A_0 wave and the S_0 wave is due to the fact that this is similar to the effect seen in experiments. The antisymmetric wave is resulting in measurements that are a couple of factors higher than the faster S_0 .



Figure 4.7: Group speed extraction of simulated signals

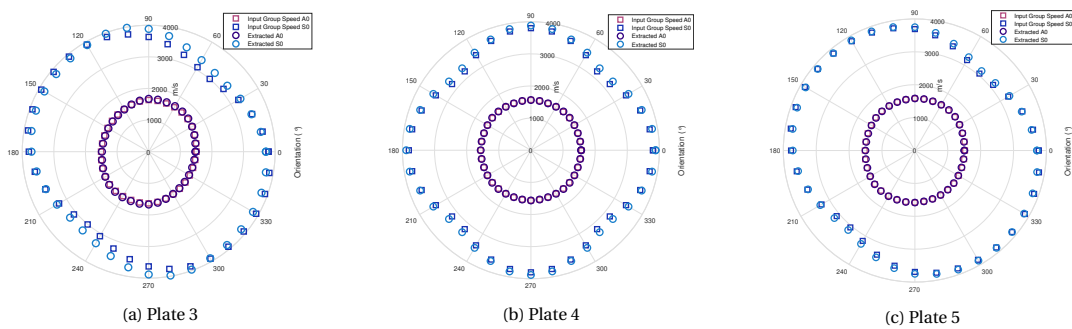


Figure 4.8: Group speed extraction of simulated signals

The group speed extracted from the simulated signals is compared with the group speed from the dispersion curve. The dispersion curve was the input to simulate the propagated signal. The score is the result of both modes (S_0, A_0), and all measured sensor orientations. The error is limited to 4 %. This is expected to be the error of the time-picking algorithm.

Plate Nr	Score	Error (%)
Plate 1	0.0777	3.28
Plate 2	0.0524	2.70
Plate 3	0.0860	3.46
Plate 4	0.0333	2.15
Plate 5	0.0144	1.41

Table 4.14: Function score of simulated signals

Figure 4.9 shows the comparison between simulated groups speeds, and the group speed extracted from the simulated sensor data. The good agreement between the simulated and the extracted results can be observed.

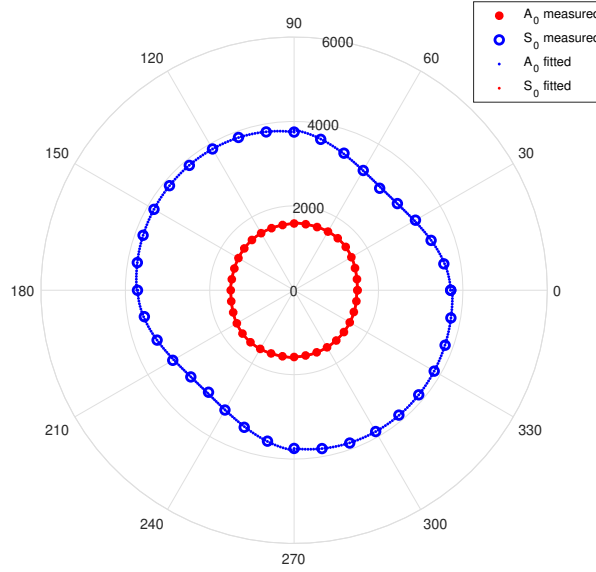


Figure 4.9: Polynomial fit through the predicted group speeds

Figure 4.10 shows all the results of the detection of the time of flight from a simulated signal. The horizontal axis shows the simulated group speed of the ultrasonic guided waves. The vertical axis shows the group speed that was acquired by analysis of the simulated measurements. In the ideal case, the points would all be on the diagonal line.

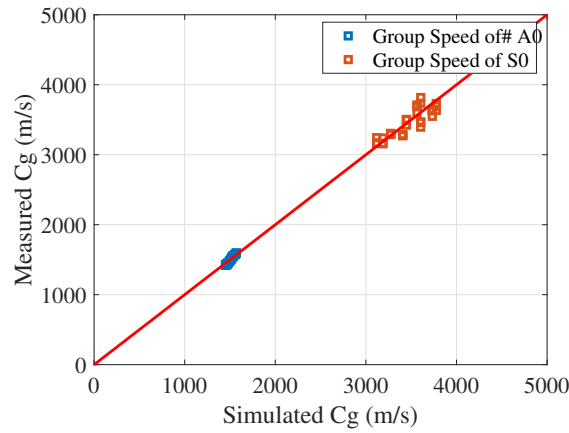


Figure 4.10: Cross correlation of extracted group speed

4.3. Measured Results

This section will show the results that have been acquired during the measurements of the actual FRC-plates as described in chapter 3. The group speeds have been extracted from the measured data using the method described in section 2.3 and curve-fitted using the method described in subsection 2.4.1. Example of raw measured signals from the experiment, are shown in Figure 4.11. The signals shown are acquired by measuring in the 0 degree direction on plate 1.1, at distances of 60, 120, 180, and 240 mm from the source, as is described in subsection 3.3.2. The arrival times of the main wave can be seen clearly from the peak values from around $240 \mu s$ to around $350 \mu s$ at sensor 1 to sensor 4, respectively.

A reflecting wave is also noticed, which has a peak in signal amplitude around $440 \mu s$ measured by sensor 4. The wave is traveling in the opposite direction from the shown time traces.

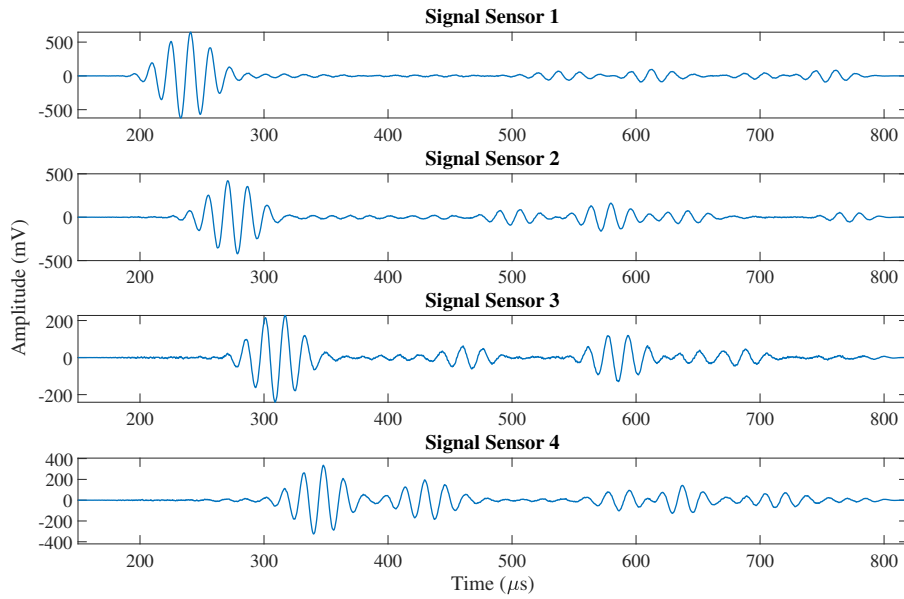


Figure 4.11: Unedited measurement

The signal analysis is performed as is described in section 2.3. This analysis is performed for every 10° orientation from the center of the plate. The results are shown in Figure 4.12 and Figure 4.13. The piece-wise polynomial fit that is created for every 90° is also included in these figures. The damping effect of the fitted curve results in a reduced effect of outliers in the group speed estimation, such as at 280° in plate 3.

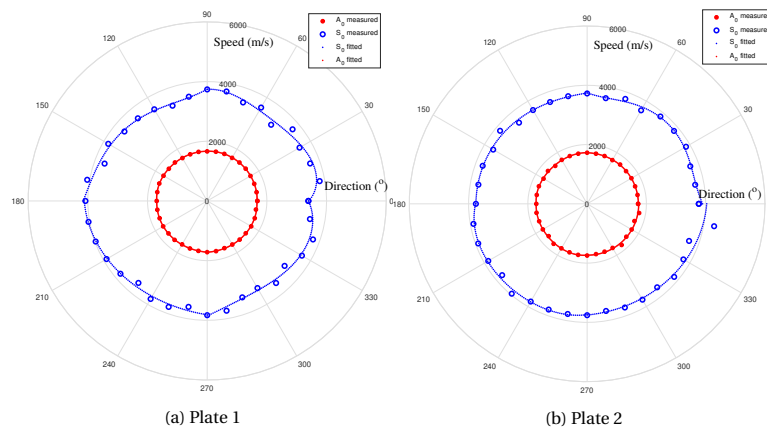


Figure 4.12: Measured group speed with polynomial curve

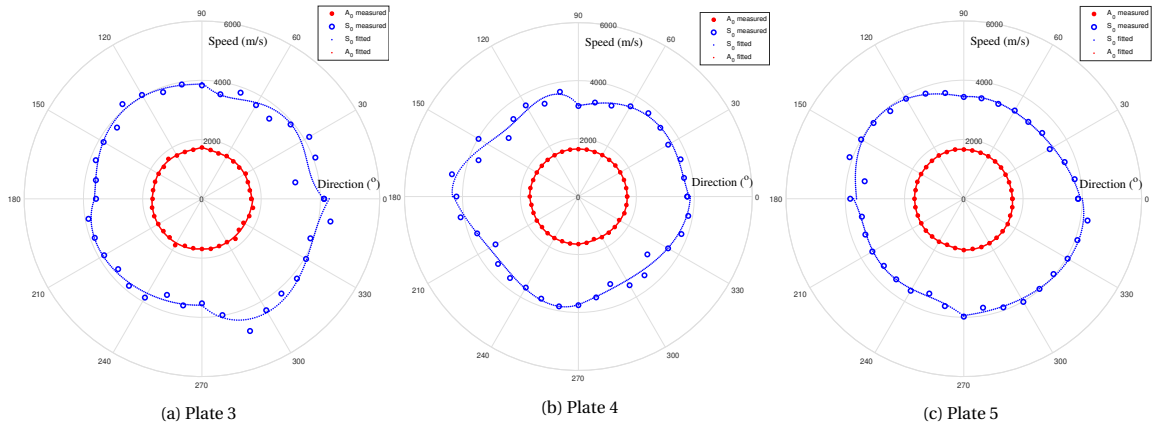


Figure 4.13: Measured group speed with polynomial curve

Next, the fitted data is used in the error minimization scheme on the measured and simulated dispersion speeds of the guided waves. The results are shown in The better fit of the antisymmetric wave that was predicted and the antisymmetric wave that was measured is noticeable. The variation of the symmetric guided wave is higher, partly due to the smaller amplitudes measured and higher uncertainty in the arrival time picking.

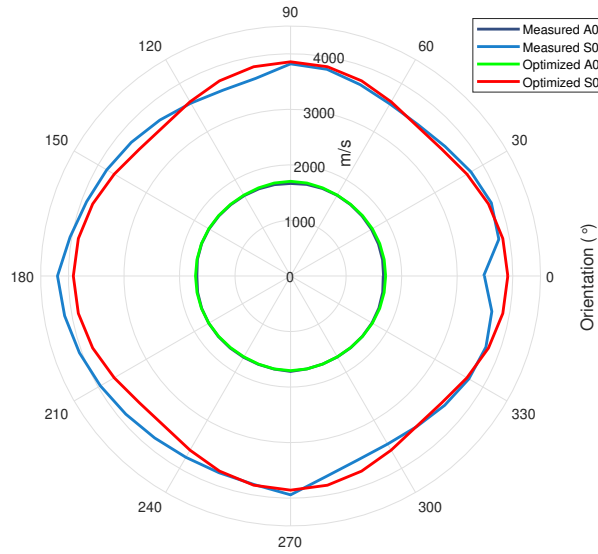


Figure 4.14: Measured and optimized polar plot of plate 1

Figure 4.15 gives a general overview of the improvement as a result of the GA. Estimating the material properties based on group speed of both modes resulted in a better correlation between estimated and measured group speeds. The effect of the optimization is that the measured group speeds are much more centralized around the diagonal, i.e., the estimated group speed is also the measured group speed. Conventional experiments are required to get a better estimation of the material properties.

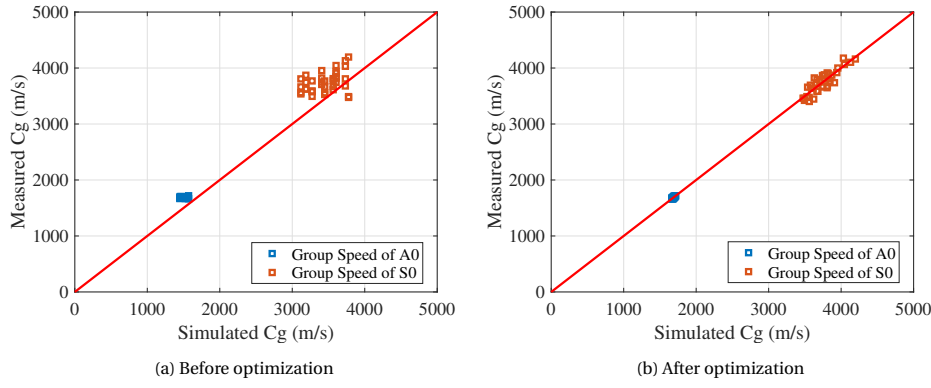


Figure 4.15: Correlation between measured and expected results

The results of the optimization can be found in section 4.4. This means the outcome of the genetic algorithm that searches for the best match between the experimental group speed and the simulated group speed.

4.4. Results from Experiment

The material estimations based of the optimization algorithms is first discussed for simulated data in subsection 4.4.1. The material estimations using the group speed acquired from measured data is shown in subsection 4.4.2.

4.4.1. Simulated Results

The estimations of the material properties based on simulated signals is shown in Table 4.15. The optimization has been performed in 24 iterations per plate. All the settings have been constant during these iterations and only the (random) starting population has changed. This is performed to show the stability of the results.

Parameter	Plate 1 Mean (COV (%))	Plate 2 Mean (COV (%))	Plate 3 Mean (COV (%))	Plate 4 Mean (COV (%))	Plate 5 Mean (COV (%))
E_{11} GPa	44.2847 (2.95)	43.1558 (5.31)	44.0459 (2.22)	50.8654 (7.21)	45.1624 (1.83)
E_{22}, E_{33} GPa	14.9180 (3.67)	15.3730 (5.74)	16.2092 (8.19)	11.9644 (17.68)	14.5500 (5.48)
ν_{12}, ν_{24} (-)	0.29	0.29	0.29	0.29	0.29
ν_{23} (-)	0.2794 (25.91)	0.3181 (28.79)	0.3590 (25.51)	0.2812 (22.86)	0.3498 (16.17)
G_{12}, G_{13} (GPa)	3.4945 (7.08)	3.2976 (8.54)	3.3769 (5.24)	4.7099 (19.43)	3.7079 (4.47)
G_{23} (GPa)	5.8226 (3.93)	5.8128 (8.66)	5.9592 (2.26)	4.6698 (17.60)	5.3889 (2.89)
ρ ($\frac{kg}{m^3}$)	1872.0	1872.0	1872.0	1872.0	1872.0
Function score	0.0883 (2.95)	0.0496 (5.13)	0.0704 (3.48)	0.0123 (6.80)	0.0203 (7.17)

Table 4.15: Plate material genetic algorithm of simulated data with fixed density and narrow Poisson's

The estimations of the material properties are familiar to the input parameters which are found in Table 4.16. The value of E_{11} has estimations which range from 3 GPa lower than expected, to values of 4.1 GPa higher than expected. It is also noted that the value of ν_{12}, ν_{13} fluctuates above and below the expected value.

Property	Input	Mean	Error %	COV (%)
E_{11} GPa	46.20	45.50	1.51	6.77
E_{22}, E_{33} GPa	13.10	14.60	11.45	10.96
ν_{12}, ν_{24} (-)	0.29	0.322	11.03	11.7
G_{12}, G_{13} (GPa)	4.10	3.724	9.20	15.49
G_{23} (GPa)	5.12	5.53	8.01	9.52

Table 4.16: Function score of simulated signals

The expected material properties are compared with the material properties, the difference between these values is determined as the error. The error between these results is between 1.51% and 11.45%. The coefficient of variation is between 6.77 % and 15.49 %.

4.4.2. Measured Results

The group speeds that belong to optimization using a GA on measured results is shown in Figure 4.16 and Figure 4.17

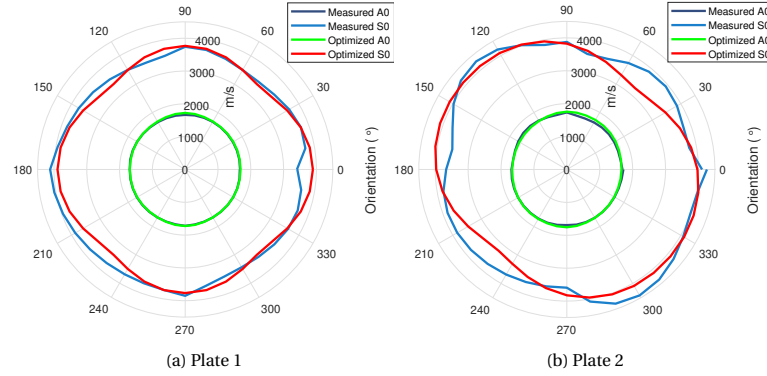


Figure 4.16: Measured group speed with polynomial curve

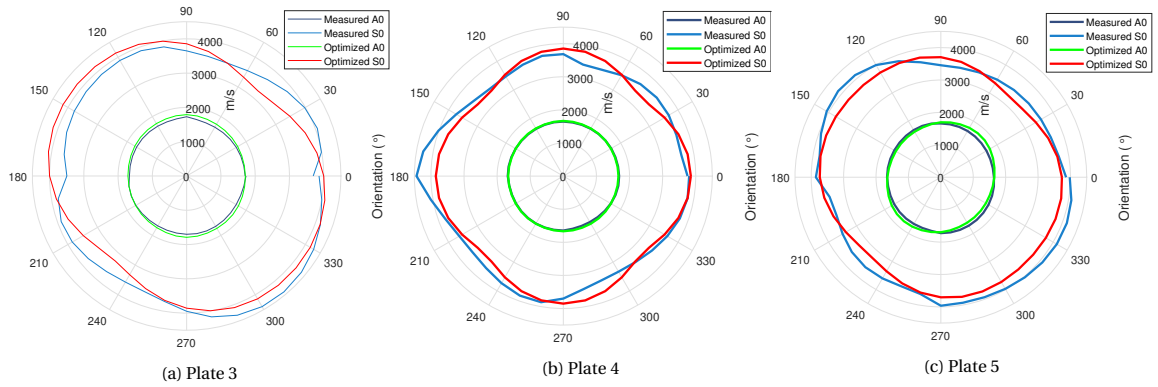


Figure 4.17: Measured group speed with polynomial curve

The results of the genetic algorithm based on the experimental data is shown in Table 4.17. The density is kept constant and known. The Poisson's ratio is also confined to the expected results for stability reasons.

The optimization has been performed in 24 iterations per plate. All the settings have been constant during these iterations and only the (random) starting population has changed. This is performed to show the stability of the results.

Parameter	Plate 1 Mean (COV (%))	Plate 2 Mean (COV (%))	Plate 3 Mean (COV (%))	Plate 4 Mean (COV (%))	Plate 5 Mean (COV (%))
E_{11} GPa	46.4818 (1.13)	51.0665 (0.58)	49.2884 (0.65)	42.7565 (3.86)	47.1832 (0.86)
$E_{22,33}$ GPa	12.1346 (4.00)	16.1419 (1.71)	16.0973 (1.80)	13.6575 (10.03)	14.9986 (2.70)
$\nu_{12,13}$ (-)	0.29	0.29	0.29	0.29	0.29
ν_{23} (-)	0.2640 (17.61)	0.4454 (2.04)	0.4440 (1.78)	0.4203 (5.06)	0.4371 (4.77)
$G_{12,13}$ (GPa)	6.1045 (1.61)	5.1589 (1.59)	5.0941 (2.11)	5.4698 (9.13)	5.1742 (2.15)
G_{23} (GPa)	4.7999 (1.01)	5.5838 (1.20)	5.5737 (1.77)	4.8048 (9.17)	5.2180 (1.94)
ρ ($\frac{kg}{m^3}$)	1872.0	1872.0	1872.0	1872.0	1872.0
Function score	0.1072 (2.67)	0.2320 (0.54)	0.2400 (0.75)	0.2819 (1.30)	0.0992 (0.61)

Table 4.17: Plate material genetic algorithm of measured data with fixed density and narrow Poisson's

The Young's modulus (E_{11}) is expected to be between 42 and 51 GPa. The values of E_{22}, E_{33} are expected to be between 12 and 16.2 GPa. The Poisson's ratio (ν_{23}) is close to the upper boundary in 4 of the 5 occasions. The Shear modulus (G_{12}, G_{13}) is estimated between 5.1 and 6.1 GPa, and 4.8 to 5.6 GPa for G_{23} .

The average error per data point is shown in Table 4.18. The score is what is minimized in the GA. A lower score is therefore a better correlation with the measured group speeds. The score is translated to a percentage error by dividing the value by all 72 measured group speeds, before taking the square root of the score. This is done because of the Least-squares approach of describing the error. The error per group speed value is between 3.7 and 6.3 %. This does however weight heavy on exceptions because of the square root in the optimization.

Plate Nr	Score	Average Error (%)
Plate 1	0.1072	3.8
Plate 2	0.2320	5.7
Plate 3	0.2400	5.8
Plate 4	0.2819	6.3
Plate 5	0.0992	3.7

Table 4.18: Function score of measured signals

The mean and coefficient of variation based on the mean values from Table 4.17 is shown in Table 4.19. Apart from the mean values, it is noted that the COV based on five plates is expected between 6 % and 20 %

Property	Mean	COV (%)
E_{11} GPa	47.3553	6.63
E_{22}, E_{33} GPa	14.0606	11.73
ν_{12}, ν_{24} (-)	0.40	19.36
G_{12}, G_{13} (GPa)	5.4003	7.77
G_{23} (GPa)	5.1960	7.47

Table 4.19: Estimation of material properties

Conclusion

It is concluded that it is feasible to determine general material properties based on the measurement of group speeds of ultrasonic guided waves. The error based on a simulated system was 11.45 % at worst, this error was made in the estimation of the value of E_{22}, E_{33} .

The estimation of material properties based on experimental data has resulted in an estimation as shown in Table 4.19.

It is concluded that it is feasible to estimate material properties using a point-contact transducer. Future research is necessary to improve the accuracy of the estimation.

An increase in measured frequencies might reduce the dependency on the correctness of the time picking algorithm. This can increase the knowledge of the dispersion curve and enrich the input data for the error minimization process. Increasing the number of measured frequencies can also result in a decrease of

measured orientations, as there is already sufficient information about the group speed of the guided wave modes, this can result in improved accuracy or better calculation efficiency.

5

Conclusion & Recommendations

Feasibility of estimation of material properties of FRC laminates using ultrasonic guided waves has been investigated in this research. Guided waves in composite laminates are multi-modal and dispersive which means that different wavemodes can travel with different speeds at different frequencies. These characteristics have been used in this research in order to estimate the properties from the measured group speeds in different directions.

The investigation comprises numerical simulations and experimental measurements. In the numerical simulations, group speed of dispersive curves in composite laminates have been constructed based on a semi-analytical approach. This method has been used in the kernel of an optimization method to translate measured group speeds from the experiments to stiffness properties of the composite laminates. In order to evaluate the methodology, five plates using different layups have been made of E-glass fibers and vinyl ester resin. These plates had dimensions of 600 x 600 x 8 mm. Dry contact transducers were used to measure guided waves, which were excited using described equipment. Wave-modes have been extracted and arrival time has been identified and translated to the speed of guided wave modes. These guided waves modes serve a central role in the created optimization algorithm based on a genetic algorithm, which is applied to the acquired data. The measured group speed of the selected wave modes had a maximum error of 6.5 %. This describes the variability of the group speed estimation.

The accuracy of the time picking of the group speed is 4 %, if based on simulated data. Material properties have been estimated based on experimental data, this results in an estimation of the Young's modulus (E_{11}) to be between 42 and 51 GPa, and the values of E_{22} , E_{33} are expected to be between 12 and 16.2 GPa. The Shear modulus (G_{12} , G_{13}) is estimated between 5.1 and 6.1 GPa, and 4.8 to 5.6 GPa for G_{23} .

The results indicate that this can be a feasible method to estimate general material properties. However, the process of time picking plays a crucial role in the determination of material properties and is recommended to be improved in future research. The band of uncertainty due to the time-picking of S0 modes is wide, which reduces the certainty of the results.

Experimental characterization of the FRC plate is crucial in order to validate the estimated material properties. Also, the proposed setup of the point-contact transducers place all sensors in a row. The experimental acquisition of the guided waves can be improved if all measurement locations are placed in the same sensor holder.

Bibliography

- D.N. Alleyne, B. Pavlakovic, M.J.S. Lowe, and P. Cawley. Rapid, long range inspection of chemical plant pipework using guided waves. In *AIP Conference Proceedings*, pages 180–187, 2001. doi: 10.1063/1.1373757. URL <http://aip.scitation.org/doi/abs/10.1063/1.1373757>.
- I. Amidror. Sub-Nyquist artefacts and sampling moiré effects. *Royal Society Open Science*, 2(3), 3 2015. ISSN 20545703. doi: 10.1098/rsos.140550.
- M. M. Ammar, Seif M. Osman, Ebtisam H. Hasan, and N. A. Azab. A tensile characterization of random glass fiber/metal laminates composites. *Materials Research Express*, 6(8):085349, 6 2019. ISSN 20531591. doi: 10.1088/2053-1591/ab2994. URL <https://iopscience.iop.org/article/10.1088/2053-1591/ab2994https://iopscience.iop.org/article/10.1088/2053-1591/ab2994/meta>.
- J. Baik and R.B. Thompson. Ultrasonic Scattering from Imperfect Interfaces: A Quasi-Static Model. Technical report, Iowa State University, 1984.
- D. Barazanchy, W. Roth, and V. Giurgiutiu. A non-destructive material characterization framework for retrieving a stiffness matrix using bulk waves. *Composite Structures*, 185:27–37, 2 2018. ISSN 02638223. doi: 10.1016/j.compstruct.2017.10.071.
- A.K. Barouni and D.A. Saravanos. A layerwise semi-analytical method for modeling guided wave propagation in laminated and sandwich composite strips with induced surface excitation. *Aerospace Science and Technology*, 51:118–141, 4 2016. ISSN 12709638. doi: 10.1016/j.ast.2016.01.023.
- M.D. Beard and M.J.S. Lowe. Non-destructive testing of rock bolts using guided ultrasonic waves. *International Journal of Rock Mechanics and Mining Sciences*, 40(4):527–536, 6 2003. ISSN 13651609. doi: 10.1016/S1365-1609(03)00027-3.
- M.G. Bellanger. *Adaptive digital filters and signal analyses*. Marcel Dekker Inc, Paris, France, second edition, 2001. ISBN 0824705637. doi: 10.1016/0165-1684(89)90053-4.
- L. A. Carlsson, D. F. Adams, and R. B. Pipes. *Experimental Characterization of Advanced Composite Materials*. CRC Press, fourth edi edition, 2014. ISBN 9781439848593. doi: 10.1201/b16618.
- composites.ugent.be. Vacuum Infusion - The Equipment and Process of Resin Infusion Introduction. Technical report, composites.ugent.be, 2020.
- A. T. Darnton and M. Ruzzene. Optical measurement of guided waves. *The Journal of the Acoustical Society of America*, 141(5):EL465–EL469, 5 2017. ISSN 0001-4966. doi: 10.1121/1.4982825. URL <http://asa.scitation.org/doi/10.1121/1.4982825>.
- C. Darwin. *On The Origin of Species*. William Collins, London, 1st editio edition, 1859. doi: 10.1017/cbo9780511693120.015.
- S. Dey, T. Mukhopadhyay, and S. Adhikari. *Uncertainty quantification in laminated composites : a meta-model based approach*. CRC Pre, 2018. ISBN 9781498784450.
- E. Egorikhina, S. V. Bogovalov, and I. V. Tronin. Determination of mechanical characteristics of unidirectional fiber composites. In *Physics Procedia*, volume 72, pages 66–72, 2015. doi: 10.1016/j.phpro.2015.09.021. URL www.sciencedirect.com.
- J. Fraser, B.T. Khuri-Yakub, and G. S. Kino. The design of efficient broadband wedge transducers. *Applied Physics Letters*, 32(11):698–700, 6 1978. ISSN 00036951. doi: 10.1063/1.89911. URL <http://aip.scitation.org/doi/10.1063/1.89911>.

- A. Ghadami, M. Behzad, and H.R. Mirdamadi. Damage identification in multi-step waveguides using Lamb waves and scattering coefficients. *Archive of Applied Mechanics*, 88:1009–1026, 2018. doi: 10.1007/s00419-018-1355-0. URL <https://doi.org/10.1007/s00419-018-1355-0>.
- V. Giurgiutiu. Lamb wave generation with piezoelectric wafer active sensors for structural health monitoring. In Amr M. Baz, editor, *Smart Structures and Materials 2003: Smart Structures and Integrated Systems*, volume 5056, page 111. SPIE, 8 2003. doi: 10.1117/12.483492. URL <http://proceedings.spiedigitallibrary.org/proceeding.aspx?doi=10.1117/12.483492>.
- S. Gopalakrishnan, A. Chakraborty, and D. Roy Mahapatra. *Spectral Finite Element Method*. Springer, 2008. ISBN 9781846283550. doi: 10.1007/978-1-84628-356-7.
- H. Gravenkamp, J. Prager, A.A. Saputra, and C. Song. The simulation of Lamb waves in a cracked plate using the scaled boundary finite element method. *The Journal of the Acoustical Society of America*, 132(3):1358–1367, 2012. ISSN 0001-4966. doi: 10.1121/1.4740478.
- M. Gresil and V. Giurgiutiu. Time-domain hybrid global-local concept for guided-wave propagation with piezoelectric wafer active sensor. *Journal of Intelligent Material Systems and Structures*, 24(15):1897–1911, 10 2013. ISSN 1045389X. doi: 10.1177/1045389X13486712.
- M.H.J. Gruber and M.H. Hayes. Statistical Digital Signal Processing and Modeling. *Technometrics*, 39(3):335, 1997. ISSN 00401706. doi: 10.2307/1271141.
- R. L. Haupt and S. E. Haupt. *Practical Genetic Algorithms Second Edition GLOSSARY*. John Wiley & Sons Inc., Pennsylvania, 2nd editio edition, 2004. ISBN 0471455652.
- T. Hayashi, C. Tamayama, and M. Murase. Wave structure analysis of guided waves in a bar with an arbitrary cross-section. *Ultrasonics*, 44(1):17–24, 1 2005. ISSN 0041624X. doi: 10.1016/j.ultras.2005.06.006.
- D.A. Hutchins, L.F. Bresse, and S.B. Palmer. Measurements with a thick conical piezoelectric transducer. *Citation: The Journal of the Acoustical Society of America*, 85:2417, 1989. doi: 10.1121/1.397790. URL <https://doi.org/10.1121/1.397790>.
- J.B. Ihn and F.K. Chang. Pitch-catch active sensing methods in structural health monitoring for aircraft structures. *Structural Health Monitoring*, 7(1):5–19, 3 2008. ISSN 14759217. doi: 10.1177/1475921707081979.
- C.H. Jenkins. *Manual on Experimental Methods of Mechanical Testing of Composites*. The Fairmont Press, 2nd editio edition, 1988. ISBN 0881732842.
- M. Kersemans, A. Martens, N. Lammens, K. Van Den Abeele, J. Degrieck, F. Zastavnik, L. Pyl, H. Sol, and W. Van Paepegem. Identification of the Elastic Properties of Isotropic and Orthotropic Thin-Plate Materials with the Pulsed Ultrasonic Polar Scan. *Experimental Mechanics*, 54(6):1121–1132, 3 2014. ISSN 17412765. doi: 10.1007/s11340-014-9861-7. URL <https://link.springer.com/article/10.1007/s11340-014-9861-7>.
- M. Kersemans, A. Martens, J. Degrieck, K. Van Den Abeele, S. Delrue, Lincy Pyl, F. Zastavnik, H. Sol, and W. Van Paepegem. The ultrasonic polar scan for composite characterization and damage assessment: Past, present and future. *Applied Sciences (Switzerland)*, 6(2):1–15, 2016. ISSN 20763417. doi: 10.3390/app6020058.
- H.W. Kim, J.K. Lee, and Y.Y. Kim. Circumferential phased array of shear-horizontal wave magnetostrictive patch transducers for pipe inspection. *Ultrasonics*, 53(2):423–431, 2 2013. ISSN 0041624X. doi: 10.1016/j.ultras.2012.07.010.
- T. Kundu, S. Das, M. Sa, and K.V. Jata. Locating point of impact in anisotropic fiber reinforced composite plates. *Struct Health Monit: Int J*, 122(4):29–45, 2007. doi: 10.1177/1475921711419991.
- H Lamb. On waves in an elastic plate. *Proceedings of the Royal Society of London. Series A, Containing Papers of a Mathematical and Physical Character*, 93(648):114–128, 3 1917. ISSN 0950-1207. doi: 10.1098/rspa.1917.0008.

- S.P. Lee, J.W. Jin, and K.W. Kang. Probabilistic analysis for mechanical properties of glass/epoxy composites using homogenization method and Monte Carlo simulation. *Renewable Energy*, 65:219–226, 5 2014. ISSN 09601481. doi: 10.1016/j.renene.2013.09.012.
- F. Li, Z. Liu, X. Sun, H. Li, and G. Meng. Propagation of guided waves in pressure vessel. *Wave Motion*, 52: 216–228, 1 2015. ISSN 01652125. doi: 10.1016/j.wavemoti.2014.10.005.
- F.M. Li, Z.G. Song, and Z.B. Chen. Active vibration control of conical shells using piezoelectric materials. *JVC/Journal of Vibration and Control*, 18(14):2234–2256, 12 2012. ISSN 10775463. doi: 10.1177/1077546311429055.
- C. Lu and W. Xu. A Model for Ultrasonic Testing Conical Transducer and Optimal Design. *Key Engineering Materials*, 467-469:801–805, 2011. doi: 10.4028/www.scientific.net/KEM.467-469.800. URL www.scientific.net.
- B.R. Mace, D. Duhamel, M.J. Brennan, and L. Hinke. Finite element prediction of wave motion in structural waveguides. *The Journal of the Acoustical Society of America*, 117(5):2835–2843, 5 2005. ISSN 0001-4966. doi: 10.1121/1.1887126.
- D.C. Malocha. *Surface Acoustic Wave (SAW) filters*. Elsevier, 2018. ISBN 9781439833230. doi: 10.1201/9781420006728.ch6.
- H. Mark and J. Workman. Calibration Transfer, Part 2: The Instrumentation Aspects. In *Chemometrics in Spectroscopy*, pages 751–764. Elsevier, 1 2018. doi: 10.1016/b978-0-12-805309-6.00102-1.
- A. Marzani and L. De Marchi. Characterization of the elastic moduli in composite plates via dispersive guided waves data and genetic algorithms. *Article Journal of Intelligent Material Systems and Structures*, 24(17): 2135–2147, 2012. doi: 10.1177/1045389X12462645.
- Mathworks. How the Genetic Algorithm Works - MATLAB & Simulink - MathWorks Benelux. URL <https://nl.mathworks.com/help/gads/how-the-genetic-algorithm-works.html>.
- J.M. Mencik and M.N. Ichchou. Wave finite elements in guided elastodynamics with internal fluid. *International Journal of Solids and Structures*, 44(7-8):2148–2167, 4 2007. ISSN 00207683. doi: 10.1016/j.ijsolstr.2006.06.048.
- P. Moilanen, P. H.F. Nicholson, V. Kilappa, S. Cheng, and J. Timonen. Measuring guided waves in long bones: Modeling and experiments in free and immersed plates. *Ultrasound in Medicine and Biology*, 32(5):709–719, 5 2006. ISSN 03015629. doi: 10.1016/j.ultrasmedbio.2006.02.1402.
- V. Munoz, M. Perrin, M. L. Pastor, H. Weleman, A. Cantarel, and M. Karama. Determination of the elastic properties in CFRP composites: Comparison of different approaches based on tensile tests and ultrasonic characterization. *Advances in Aircraft and Spacecraft Science*, 2(3):249–261, 2015. ISSN 22875271. doi: 10.12989/aas.2015.2.3.249. URL <http://dx.doi.org/10.12989/aas.2015.2.3.249>.
- P.B. Nagy, F. Simonetti, and G. Instanes. Corrosion and erosion monitoring in plates and pipes using constant group velocity Lamb wave inspection. *Ultrasonics*, 54:1832–1841, 2014. doi: 10.1016/j.ultras.2014.01.017. URL <http://dx.doi.org/10.1016/j.ultras.2014.01.017>.
- J. A. Nelder and R. Mead. A Simplex Method for Function Minimization. *The Computer Journal*, 7(4):308–313, 1 1965. ISSN 0010-4620. doi: 10.1093/comjnl/7.4.308. URL <https://academic.oup.com/comjnl/article-lookup/doi/10.1093/comjnl/7.4.308>.
- W. Ostachowicz, P. Kudela, M. Krawczuk, and A. Zak. *Guided Waves in Structures for SHM: The Time-Domain Spectral Element Method*. Wiley, 2012. ISBN 9780470979839. doi: 10.1002/9781119965855.
- L.P. Pahlavan. *Wave Propagation in Thin-walled Composite Structures: Application to Structural Health Monitoring*. TU Delft, Delft, 2012. ISBN 978-94-6203-267-5.
- M. Ponschab, D.A. Kiefer, and S.J. Rupitsch. Towards an Inverse Characterization of Third Order Elastic Constants Using Guided Waves. In *IEEE International Ultrasonics Symposium, IUS*, pages 1264–1268. IEEE Computer Society, 10 2019. ISBN 9781728145969. doi: 10.1109/ULTSYM.2019.8926294.

- C Radhakrishna Rao and Helge Toutenburg. *Linear Models: Least Squares and Alternatives*. Springer, New York, 2nd editio edition, 1999. ISBN 0-387-98848-3. doi: 10.2307/2965595.
- P. Ragauskas and R. Belevicius. Identification of material properties of composite materials. *Aviation*, 13(4): 109–115, 2009. ISSN 16487788. doi: 10.3846/1648-7788.2009.13.109-115.
- J.L. Rose. *Ultrasonic guided waves in solid media*. Cambridge University Press, Pennsylvania, 2014. ISBN 9781107048959.
- G. Rus, S. Wooh, and R. Gallego. Design of ultrasonic wedge transducer. *Ultrasonics*, 43:391–395, 2005. doi: 10.1016/j.ultras.2004.10.002. URL www.elsevier.com/locate/ultras.
- G. Rus, S.C. Wooh, and R. Gallego. Processing of ultrasonic array signals for characterizing defects. Part II: Experimental work. *IEEE Transactions on Ultrasonics, Ferroelectrics, and Frequency Control*, 54(10):2139–2145, 2007. ISSN 08853010. doi: 10.1109/TUFFC.2007.509.
- M. Sale, P. Rizzo, and A. Marzani. Semi-analytical formulation for the guided waves-based reconstruction of elastic moduli. *Mechanical Systems and Signal Processing*, 25(6):2241–2256, 8 2011. ISSN 08883270. doi: 10.1016/j.ymsp.2011.02.004.
- M.S. Salmanpour, Z. Sharif Khodaei, and M.H. Aliabadi. Transducer placement optimisation scheme for a delay and sum damage detection algorithm. *Structural Control and Health Monitoring*, 24(4), 4 2016. ISSN 15452263. doi: 10.1002/stc.1898.
- M.G.R. Sause, M.A. Hamstad, and S. Horn. Finite element modeling of conical acoustic emission sensors and corresponding experiments. *Sensors and Actuators, A: Physical*, 184:64–71, 9 2012. ISSN 09244247. doi: 10.1016/j.sna.2012.06.034.
- Seartex GmbH Co. KG. SAERTEX material calculator, 2013. URL <https://www.saertex.com/en/products/material-calculator>.
- L. Sun, W. Li, Y. Wu, and Q. Lan. Active vibration control of a conical shell using piezoelectric ceramics. *Journal of Low Frequency Noise, Vibration and Active Control*, 36(4):366–375, 12 2017. ISSN 1461-3484. doi: 10.1177/1461348417744304. URL <http://journals.sagepub.com/doi/10.1177/1461348417744304>.
- J. F. Tressler, S Alkoy, and R. E. Newnham. Piezoelectric sensors and sensor materials. *Journal of Electroceramics*, 2(4):257–272, 1998. ISSN 13853449. doi: 10.1023/A:1009926623551. URL <https://link.springer.com/article/10.1023/A:1009926623551>.
- Vallen System. AMSY-6 System Specification, 2020a. URL <http://www.vallen.de>.
- Vallen System. AE-Preamplifier Data Sheet, 2020b. URL https://www.vallen.de/wp-content/uploads/2019/03/Datasheet_AEP3N_1602.pdf.
- J. Vishnuvardhan, C.V. Krishnamurthy, and K. Balasubramaniam. Genetic algorithm based reconstruction of the elastic moduli of orthotropic plates using an ultrasonic guided wave single-transmitter-multiple-receiver SHM array. *Smart Materials and Structures*, 16(5):1639–1650, 8 2007. ISSN 0964-1726. doi: 10.1088/0964-1726/16/5/017.
- M. Webersen, S. Johannesmann, J. DÜchting, L. Claes, and B. Henning. Guided ultrasonic waves for determining effective orthotropic material parameters of continuous-fiber reinforced thermoplastic plates. *Ultrasonics*, 84:53–62, 3 2018. ISSN 0041624X. doi: 10.1016/j.ultras.2017.10.005.
- Q. Xie, C. Ni, and Z. Shen. Defects detection and localization in underwater plates using laser laterally generated pure non-dispersive S0 mode. *Applied Sciences (Switzerland)*, 9(3), 1 2019. ISSN 20763417. doi: 10.3390/app9030459.
- G. G. Yen and K. C Lin. Wavelet packet feature extraction for vibration monitoring. *IEEE Transactions on Industrial Electronics*, 47(3):650–667, 2000. ISSN 02780046. doi: 10.1109/41.847906.

- M. Zhao, L. Zeng, J. Lin, and W. Wu. Mode identification and extraction of broadband ultrasonic guided waves. *Measurement Science and Technology*, 25(11):115005, 11 2014. ISSN 13616501. doi: 10.1088/0957-0233/25/11/115005. URL <https://iopscience.iop.org/article/10.1088/0957-0233/25/11/115005><https://iopscience.iop.org/article/10.1088/0957-0233/25/11/115005/meta>.
- A.A. Zul Karnain and P. Rajagopal. Effect of Conical Profile on the Transmission of Elastic Waves From Cylindrical Waveguide to Bulk. *Journal of Nondestructive Evaluation, Diagnostics and Prognostics of Engineering Systems*, 3(3), 8 2020. ISSN 2572-3901. doi: 10.1115/1.4046724.
- P. Zuo, X. Yu, and Z. Fan. Numerical modeling of embedded solid waveguides using SAFE-PML approach using a commercially available finite element package. *NDT and E International*, 90:11–23, 9 2017. ISSN 09638695. doi: 10.1016/j.ndteint.2017.04.003.